Master's Thesis

Solar Light Assisted Reductive Hydrogen Peroxide Production from Dioxygen and Water

Yerin Hong

Department of Chemical Engineering

Graduate School of UNIST

2019

Solar Light Assisted Reductive Hydrogen Peroxide Production from Dioxygen and Water

Yerin Hong

Department of Chemical Engineering

Graduate School of UNIST

Solar Light Assisted Reductive Hydrogen Peroxide Production from Dioxygen and Water

A thesis
submitted to the Graduate School of UNIST
in partial fulfillment of the
requirements for the degree of
Master of Science

Yerin Hong

06. 11. 2019 of submission
Approved by

Advisor
Ji-Wook Jang

Solar Light Assisted Reductive Hydrogen Peroxide Production from Dioxygen and Water

Yerin Hong

This certifies that the thesis of Yerin Hong is approved.

06. 11. 2019 of submission

Advisor: Ji-Wook Jang

Changduk Yang

Hoi Ri Moon

Abstract

The finite nature of fossil fuel reserves and the increasing pace of climate change mean that we must find and harness clean and sustainable energy sources. H_2O_2 can be one such energy source as it generates more energy than any other fuel without generating any pollutant. Moreover, H_2O_2 has widespread applications in chemical industries, medicinal science, water treatment, etc. However, the commercial multistep anthraquinone (AQ) process for H_2O_2 production requires high energy input for hydrogenation/oxidation reaction, gases supply (H_2 and O_2), and noble metal catalysts. The usage of organic solvents and generation of by-products during extraction makes it non-eco-friendly process. However, photocatalytic H_2O_2 generation can be a potential replacement to AQ process, as it doesn't require explosive hydrogen gas, expensive noble metals, etc. Considering, H_2O_2 as a potential future energy carrier, the research will be much focused on constructing an efficient and sustainable photochemical solar H_2O_2 production system capable of producing high concentrations of H_2O_2.

In this dissertation, three different potential light absorbers (pristine as well as hybrid) have been synthesized directly/ indirectly to construct a sustainable powder based photocatalytic system capable of producing high concentrations of H_2O_2 under visible light irradiation at ambient conditions. In this reported research work, both organic as well as inorganic photocatalysts have been utilized to scale up the H_2O_2. In Chapter 2, to maximize the light harvesting efficiency over a wide range of the solar spectrum and enhancing the charge transfer efficiency by minimizing charge recombinations, polymer/TiO_2 heterojunction photocatalyst has been synthesized. To find an ideal combination, and to construct an efficient heterojunction between poly (fluorene-benzothiadiazole) (PFBT) based polymeric photocatalyst and TiO_2, three different fluorine substituted PFBT polymer (PFBT, PFFBT, and PF2FBT) have been synthesized and tested. Compared to bare TiO_2, polymer/TiO_2 heterojunction (polymer having 1 or 2 fluorine atom) generates nearly 80 times higher H_2O_2. The theoretical calculations corroborated by experimental results demonstrate that the hydrophobic character of the polymeric photocatalysts plays a key role in maximizing the performance of polymer/TiO_2 hybrid catalyst. The hydrophobic character of fluorinated PFBT polymeric photocatalysts restricts the surface adsorption of photogenerated H_2O_2, which prevent the photodegradation of the same. Contrary to polymer/TiO_2 heterojunction polymer, bare TiO_2 show a high degree of H_2O_2 photodegradation which highlights its inability of H_2O_2 production in the absence of surface shielding. The hydrophobic nature of pristine polymeric, as well as hybrid photocatalysts, have been substantiated by contact angle measurement studies.

As we highlighted earlier, one of the main challenges for scale up the photochemical H_2O_2 generation is the stabilization of photogenerated H_2O_2 in the reaction medium. In Chapter 3, the metal-organic framework (MOF) derived carbon encapsulated CdS (C@CdS) composite photocatalysts have been synthesized and tested for photochemical H_2O_2 generation. The C@CdS photocatalyst is synthesized by carbonization of cadmium and sulfur atoms containing MOF by annealing at the high temperature in different gases environment. The transformation of MOF structure to C@CdS photocatalyst has been confirmed by analysis-ray diffraction, and electron microscopic techniques. The carbon matrix on the surface of CdS photocatalyst act as a shield to inhibiting the H_2O_2 photodecomposition on its surface. The exciting feature of this reported work is the unassisted (i.e., in the absence of hole scavenger) H_2O_2 production under visible light irradiation. The encapsulation of CdS into the carbon matrix increases the H_2O_2 production (2 mM) by nearly 4 folds in comparison to commercialized CdS. The extended photochemical reaction studies demonstrate the absence of point of equilibration even after 24 h irradiation in the case of for C@CdS which further widened the difference in the photogenerated H_2O_2 concentration over C@CdS (2.09 mM) and commercial CdS (0.33 mM) after 24 h of visible light irradiation.

In Chapter 4, organic photocatalyst graphitic carbon nitride (g-C_3N_4) has been utilized for photochemical production of H_2O_2. To carry out the photochemical reaction g-C_3N_4 was synthesized by ionothermal process. The optimized ionothermal method helps us in synthesizing triazine structured, highly photoactive g-C_3N_4. A comparison has also been drawn between the photochemical H_2O_2 generation efficiency of g-C_3N_4 sample synthesized by two different methods, i.e., thermal condensation, and ionothermal process. It was quite surprising that g-C_3N_4 synthesized by ionothermal process shows nearly 7 fold high H_2O_2 production (16 mM) after 24 h of visible light irradiation under ambient conditions. The H_2O_2 production rate over as-synthesized g-C_3N_4 is far higher than any of the photochemical processes reported so far, and even comparable to the electrochemical processes for H_2O_2 production.

Contents

2. Solar Light Assisted Reductive Hydrogen Peroxide Production by Polymer/TiO_2 heterojunction Photocatalyst from Dioxygen and Water

3. Solar Light Assisted Reductive Hydrogen Peroxide Production by MOF-Derived Carbon@CdS Photocatalyst from Dioxygen and Water

4. Solar Light Assisted Reductive Hydrogen Peroxide Production by Graphitic Carbon Nitride photocatalyst from Dioxygen and Water

List of Tables

List of Figures

List of List of Abbreviations

AO	Anthraquinone Oxidation
AQ	Anthraquinone
CB	Conduction Band
DFT	Density Functional Theory
DMF	*N*,*N*-dimethylformamide
DPPFC	Direct Peroxide/Peroxide Fuel Cell
EDDA	Ethylenedithiodiacetic acid
EDS	Energy-dispersive X-ray Spectroscopy
FT-IR	Fourier-Transform Infrared Spectroscopy
HOMO	Highest Occupied Molecular Orbital
HR-TEM	High-Resolution Transmission Electron Microscopy
LUMO	Lowest Un-occupied Molecular Orbital
MOF	Metal-Organic Framework

NHE	Normal Hydrogen Electrode
NIR	Near Infra-Red
PEC	Photoelectrochemical
PFBT	Poly (fluorene-benzothiadiazole)
PL	Photoluminescence
PTFE	Polytetrafluoroethylene
PV	Photovoltaic
SEM	Scanning Electron Microscope
SHE	Standard Hydrogen Electrode
TGA	Thermogravimetric Analysis
UV	Ultra Violet
VB	Valence Band
Vis	Visible
XPS	X-ray Photoelectron Spectroscopy
XRD	X-ray Diffraction

Solar Light Assisted Reductive Hydrogen Peroxide Production from Dioxygen and Water

1. General Introduction

1.1. Hydrogen peroxide

1.1.1. Introduction

Hydrogen peroxide (H_2O_2) is considered as one of the best oxidizing materials that is environmentally benign because of it only release unharmful byproduct, water, after redox process [1]. In the list of the 100 most important chemical compounds, hydrogen peroxide was listed one of them [2]. The application field of hydrogen peroxide is diverse such as a pulp and paper bleaching agent, disinfectant, detergent, chemical synthesis, textile industry, electronics industry [3]. Hydrogen peroxide is also used to treat wastewater or industrial waste. It can remove diverse kinds of materials in wastes by oxidation. For example, cyanide, thio-cyanate, nitrite, chloride, hypochlorite, and other organics can be degraded through oxidation process [4]. It is also considered as a good energy-storage medium because it is liquid phase and its stability and portability are better comparing with a gas phase energy-storage materials such as hydrogen gas [5]. Moreover, hydrogen peroxide has a high energy density and it can be utilized in a fuel cell such as direct peroxide/peroxide fuel cell (DPPFC) to produce of electricity [6]. The energy density of 60% of aqueous hydrogen peroxide by volume is 3.0MJ/L and the energy density of it by weight is 2.1 MJ/Kg. Since the energy density of compressed hydrogen gas (35MPa) is 2.8MJ/L and 3.5MJ/kg respectively, H_2O_2 can be considered as a comparable energy carrier to hydrogen [7]. Market size of hydrogen peroxide in U.S was 3.89 billion dollars in 2015 and, it is estimated to grow more than 5% by 2024 and at that time, the requirement of hydrogen peroxide will be increased in all fields [8]. Not only U.S.A, but other continents consume hydrogen peroxide with large quantity. Especially, more than half of hydrogen peroxide was demanded in Asia Pacific region [9].

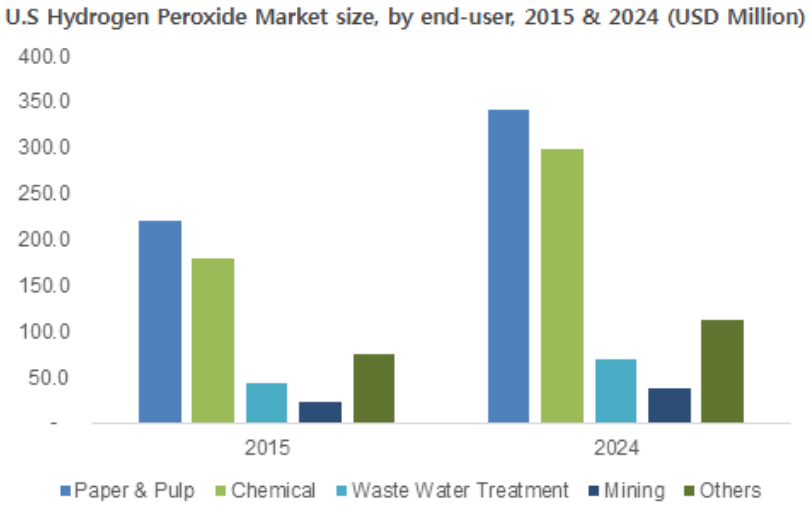

Figure 1.1. U.S hydrogen peroxide market size in 2015 and 2024 [8].

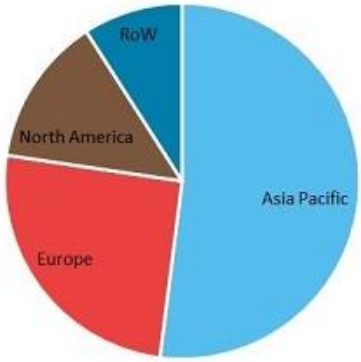

Figure 1.2. Global hydrogen peroxide demand by region [9].

1.1.2. Industrial hydrogen peroxide production

Currently, the main process that hydrogen peroxide is produced industrially is called anthraquinone oxidation (AO) process [10]. In the AO process, oxidized anthraquinone is reduced by hydrogen gas and a noble metal catalyst such as palladium (Pd) is utilized in the process. Then reduced anthrahydroquinone is produced and it is oxidized to anthraquinone by reacting with oxygen gas. During the oxidation of anthrahydroquinone to anthraquinone, hydrogen peroxide is generated by the reduction of the oxygen gas. Even though the AO process is proper for forming a high concentration of H_2O_2 with large quantity, there are several weaknesses. First, the process occurs a hydrogenation reaction of the unsubstituted aromatic ring and result in the creation of

tetrahydroanthrahydroquinone as a byproduct. In this case, the regeneration process of both catalyst and solution is required. Second, the additional separation steps of H_2O_2 from other organic impurities are included in the AO process [11]. Third, hydrogen/oxygen gas mixture is needed and it has the danger of explosion [12]. Fourth, the palladium catalyst is used in the AO process and the high price of noble metal is one of the burdens of the AO process. One time, Pd catalyst was alternatives of noble platinum (Pt) catalyst because of its lower cost than that of Pt. However, the current price of Pd is much higher than the price of Pt [13]. Finally, anthraquinone solvent is toxic thus causes environmental problems and to extract H_2O_2, this process requires high energy input.

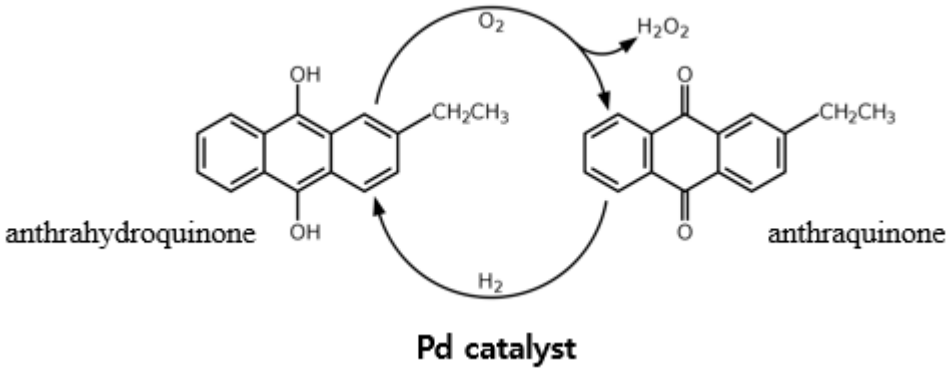

Figure 1.3 Comertialized anthraquinone oxidation (AO) process for hydrogen peroxide production.

1.1.3. Another process for hydrogen peroxide production

The conventional hydrogen peroxide production results in many problems. Thus, other methods to produce hydrogen peroxide is developing. One of them is the direct synthesis of hydrogen peroxide by palladium catalyst. The AO process is indirect synthesis for H_2O_2 that needs the hydrogenation step of anthraquinone and oxidation step of anthrahydroquinone. Therefore, a simple direct synthesis process of H_2O_2 from H_2 and O_2 is establishing although it is not commercialized method and hard to get a large quantity of H_2O_2 yet. The noble metal palladium catalyst is known for good at oxidizing H_2 but produced hydrogen peroxide easily decomposed to water due to its unstable property. To maintain hydrogen peroxide concentration, halide and acid are required in this process. To acquire competitiveness to conventional AO process, the selectivity of H_2 of the direct synthesis process have to increase up to 95 % [14]. Other production methods such as a direct reaction of H_2 and O_2 on novel metal catalysts, and electrocatalysis, and photoelectrochemical production are still

developing process. However, the direct synthesis requires noble metal catalyst and still use H_2/O_2 gas mixture, so there is danger of explosion. In case of the electrocatalysis, H_2O_2 can generated in cathode part by reducing the oxygen gas but counter electrode is usually noble metal catalyst such as a platinum and this process requires expensive substrate such as FTO or ITO and materials. Moreover, electrochemical synthesis requires additional energy input. Thus, photocatalysis can be a potential alternative to generate hydrogen peroxide to solve these problems.

1.2. Photocatalyst

1.2.1. Needs for renewable energy

The importance of renewable energy is getting bigger because of the depletion of fossil fuels and environmental problems. The coal, natural oil, and gas are not a sustainable energy source and it will be exhausted in the end. Besides, to utilize fossil fuels, carbon dioxide is fatally emitted because fossil fuels are mainly composed of hydrocarbon and the combustion process of fossil fuels makes carbon be oxidized. Carbon dioxide is the gas phase material that leads to global warming. United Nations Climate Change Conference in Paris in 2015 made an agreement with reducing the emission of greenhouse gases. Thus, environmental regulation by government is predicted to be stricter with the course of time. However, the human population is still increasing and requirements of energy and energy infrastructure also rise.

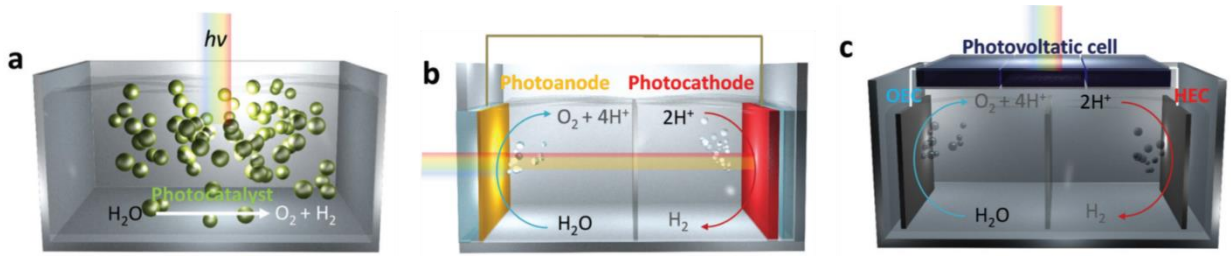

Figure 1.4. Solar energy devices a) Particulate photocatalytic water splitting system, b) Photoelectrochemical (PEC) water splitting system and c) Photovoltaic–photoelectrochemical hybrid (PV–PEC) system [15].

Renewable energy can be a solution to these problems. It includes solar energy, biomass, wind energy, geothermal energy, tide energy, etc. Renewable energy has no danger of depletion and it

doesn't produce pollutants or carbon dioxide that is harmful to both human and environment. Among them, solar energy is the key to a clean energy source. It is an abundant, inexhaustible and delocalized energy source. Many devices have been developed for capture, conversion, and storage of it [16]. For example, Photovoltaic (PV) is a device that converts light to electricity and the solar cell is a one of PV cell using solar light as a light source. Photoelectrochemical cell, artificial photosynthesis, and photocatalyst are other devices that utilize solar energy to generate solar fuels. **Figure 1.4** describes three types of solar device. Photocatalytic solar fuel production (**Figure 1.4a**), photoelectrochemical solar fuel production (**Figure 1.4b**) and Photovoltaic–photoelectrochemical solar fuel production (**Figure 1.4c**).

1.2.2. Introduction to photocatalyst

Photocatalysts are semiconductor materials that have proper band gap generating photoexcited electrons and hole by solar radiation. Metal oxides, metal nitrides, and metal sulfides are usually used as photocatalysts. When photocatalyst absorbs light, electron-hole pairs are generated by the photoelectric effect. Then, two carriers are separated. Electrons move to the conduction band and holes move to the valence band and both transfer to the surface of the photocatalyst. Electrons participate in the reduction reaction of adsorbed reactants and holes participate in the oxidation reaction of adsorbed reactant. **Figure 1.5** describes the basic mechanism of photocatalytic water splitting.

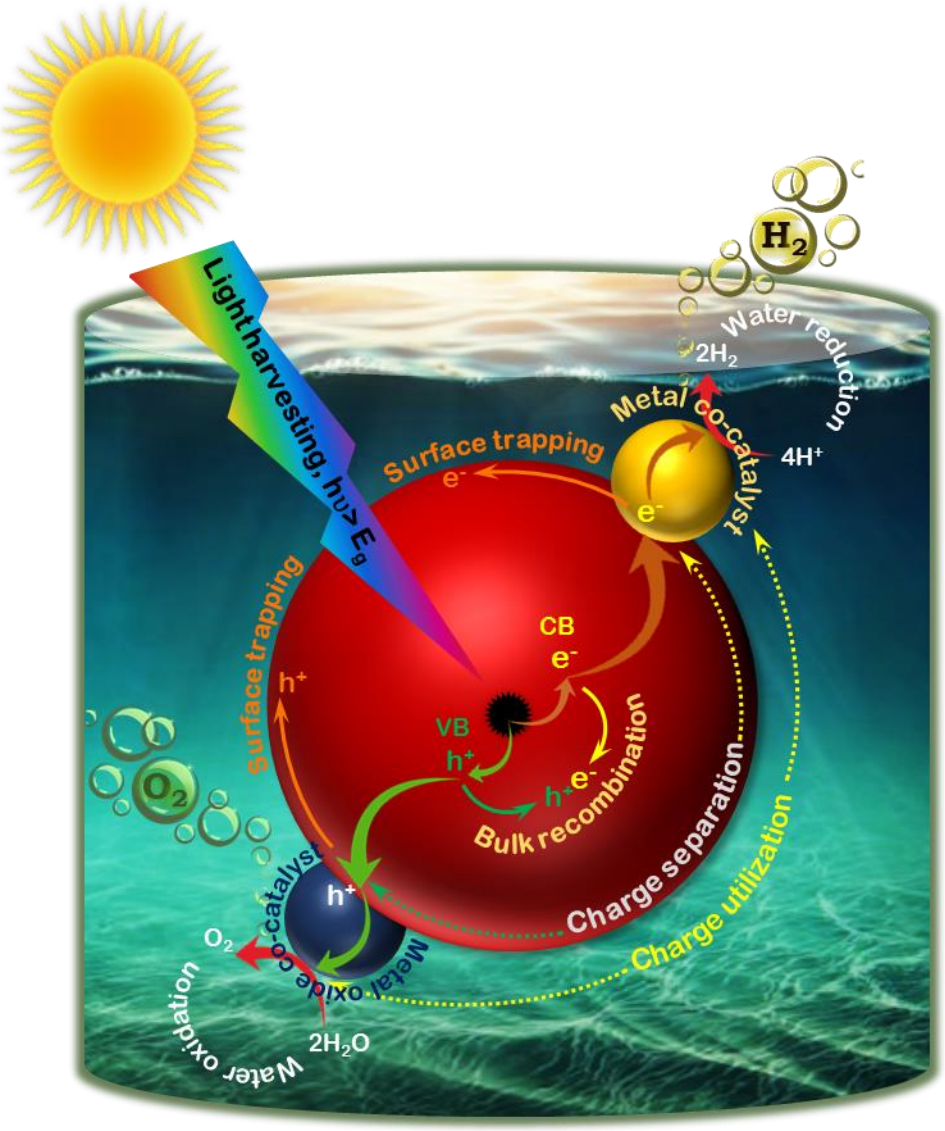

Figure 1. 5. Schematic representation of general phenomena on a photocatalyst such as light harvesting, photo excitation, charge carrier generation (h^+ and e^-), charge separation, charge diffusion, charge recombination, charge utilization (water splitting/chemical conversion), co-catalysts for fast charge transfer, and surface trapping.

Photocatalysts usually applied in two fields. Firstly, the photocatalyst is used for environmental treatment such as water or air cleaning by decomposing organic and inorganic contaminants. Secondly, it is used to convert and store solar energy to chemical energy by producing chemical fuel such as hydrogen gas or oxygen gas. Main products from photocatalyst are hydrogen

gas [17, 18] and oxygen gas [19, 20] by splitting water. Hydrogen is a clean energy carrier and used as fuel. Hydrogen is mainly produced by steam reforming in this process, methane and steam (gas phase H_2O) is reacted in presence of nickel catalyst. Final products are carbon dioxide gas and hydrogen gas. Although it is great process to generate hydrogen with high yield (65 ~ 75 % of efficiency), it consumes methane that is also fuels and produce greenhouse gas. Thus, photocatalyst is good candidate for producing hydrogen with eco-friendly way. In case of the photocatalyst, hydrogen is formed from reduction of water by photogenerated electrons and oxygen is formed from oxidation of water by photogenerated holes. However, not all materials can be applied to generate chemicals from the sun light. For hydrogen evolution reaction (HER), conduction band should be positioned above of the H_2O/H_2 energy level (0.0 V vs. NHE at pH=7) and valence band should be positioned below of the O_2/H_2O energy level (1.23 V vs. NHE at pH=7) at the same time. In addition, considering overpotential, at least 1.6 eV of band gap size is required. Figure 1.6 shows variety band gap of photocatalysts. Conduction bands of some semiconductors (e.g. MoS_2, WO_3 and Fe_2O_3) are below the 0.0 V (H_2O/H_2) so it is impossible to generate hydrogen gas. Otherwise, GaAs and InP are unsuitable to produce oxygen gas because valence bands of them are above 1.23 V (O_2/H_2O).

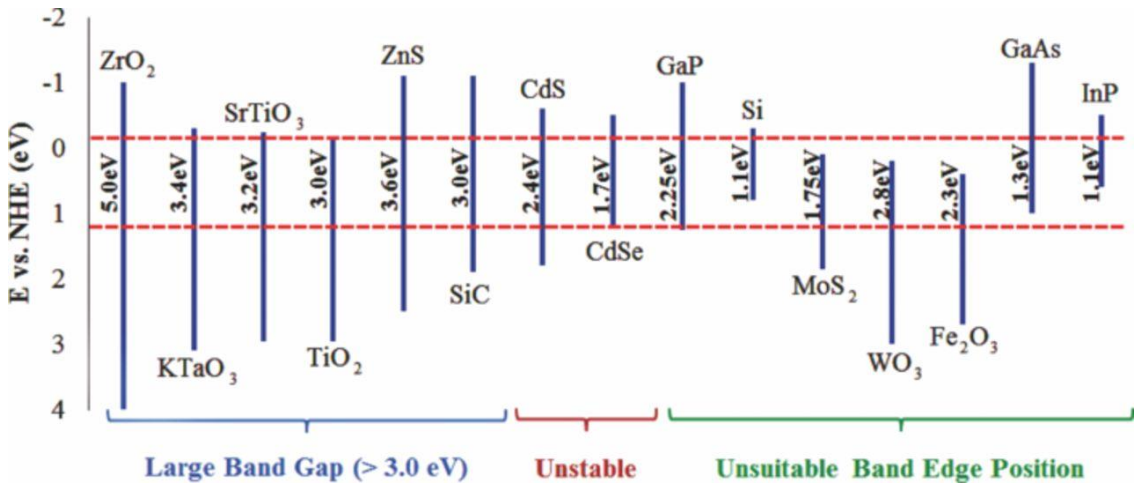

Figure 1.6. Band-gap structure of some semiconductors and their limitations for water splitting [21].

Other reaction such as carbon dioxide reduction to fuels [22], nitrogen fixation to ammonia [23], and generation of hydrogen peroxide [24] can be conducted using photocatalysts. Reducing the CO_2 is one of the important issues for the environment. By using photocatalysts, CO_2 can be transformed to chemical fuels such as methanol, methane or formate. This technique helps to decrease CO_2 and reuse fuels again. Nitrogen fixation is the process that converts nitrogen in the atmosphere to ammonia or

other nitrogen-containing chemicals. It is essential because nitrogen is used for fertilizer. In nature, nitrogen-fixing bacteria can carry this process out. Today, the Haber-Bosch process is industrial nitrogen fixation process and it produces ammonia from the nitrogen. However, it needs high temperature (400 ~ 500 ºC) and high pressure (150 ~ 250 atm). Photocatalytic production of ammonia, however, can generate it with ambient temperature and pressure. Photocatalytic hydrogen peroxide production also has several advantages compared to the industrial process.

1.2.3. Photocatalytic production of hydrogen peroxide

As mentioned above (in **Chapter 1.1.2**), various problems arise from the generation of commercialized hydrogen peroxide. However, photocatalytic production of H_2O_2 can be a solution to these problems. Photo-driven hydrogen peroxide production has several advantages over the pre-existing process. It does not require explosive H_2 gas because hydrogen peroxide can be generated by reducing oxygen gas (0.695 V vs. NHE) through photoexcited electrons or by oxidizing water (1.763 V vs. NHE) through photoexcited holes. This process can be achieved in the presence of only solar energy, water and oxygen and all of these are abundant resources in the Earth. Moreover, this process is not needed high energy input like high pressure or temperature and an expensive metal catalyst. However, H_2O_2 is a chemical that widely used as a hole removing agent in the photocatalytic reaction. It indicates that produced H_2O_2 can be easily decomposed by the photoexcited holes on the surface of the photocatalyst when is adsorbed on the photocatalyst. Therefore, maintaining a high concentration of hydrogen peroxide is an important issue in this field.

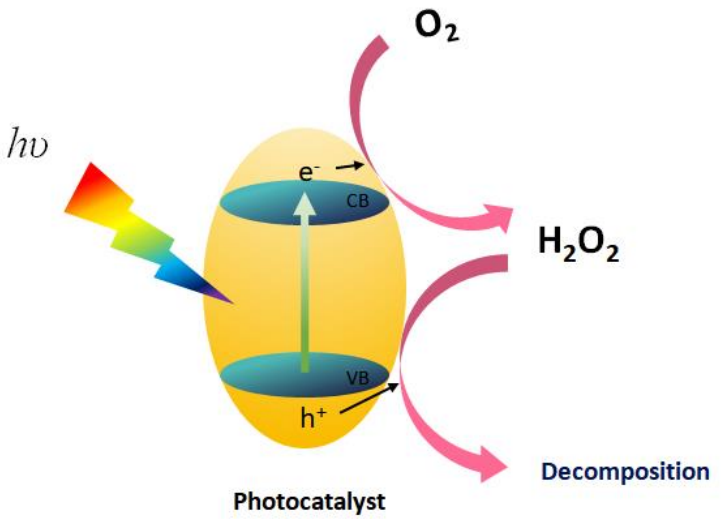

Figure 1.7. Schematic illustration of H_2O_2 generation by photocatalyst *via* oxygen reduction

1.3. Scope and objective of the work

To scale-up the H_2O_2 production generated by photocatalytic method, we can consider several development process. For example, the activity of the photocatalysts itself can be enhanced by doping for band gap engineering, or loading co-catalyst for fast charge separation and better selectivity. Otherwise, the concentration of the H_2O_2 can be increased by preventing the photodecomposition of generated hydrogen peroxide by inhibiting the adsorption of it on the surface of the photocatalyst. My two researches are focus on the preventing adsorption of the hydrogen peroxide and minimizing its photodecomposition while main goal of a last research is concentrated on enhancing the activity of the photocatalyst. Frist work avoids degradation of hydrogen peroxide by synthesizing a photocatalyst that has hydrophobic nature. Second work avoids degradation of hydrogen peroxide by encapsulating a photocatalyst with carbon matrix. Third work improves photoactivity by synthesizing a photocatalyst more crystalline thorough different synthesis method. In all the cases, the concentration of the hydrogen peroxide is dramatically increased.

1.4. Outline of this dissertation

In here, three different photocatalysts are introduced for hydrogen peroxide production under ambient temperature and pressure from earth-abundant resources. One is polymer/TiO_2 organic/inorganic heterojunction powders (in **Chapter 2**). It is suitable photocatalyst under visible light although TiO_2 itself don't active under visible light because polymer has a short band gap and heterojunction with polymer helps to absorb longer wavelength. In addition, the hydrophobic property of polymer inhibits decomposition of hydrogen peroxide. Another is directly synthesized carbon@CdS composite from MOF structure (in **Chapter 3**). This catalyst not only generates a high concentration of hydrogen peroxide than commercial CdS but also carbon on the surface of CdS helps to block degradation of produced hydrogen peroxide. The other is crystalline graphitic carbon nitride powders synthesized through ionothermal polymerization (in **Chapter 4**). Crystalline and condensed graphitic carbon nitride shows exceptional performance than bulk carbon nitride. As my knowledge, it is the highest value among reported papers about photocatalytic hydrogen peroxide production. All the photocatalysts well applied under the visible light condition and especially, polymer/TiO_2 and carbon@CdS can be applied to a system that does not requires sacrificial agent.

1.5. References

[1] Yi, Y., Wang, L., Li, G. & Guo, H. *Catalysis Science & Technology* 6, **2016**, 1593–1610.

[2] R. L. Myers, The 100 most important chemical compounds: a reference guide, Greenwood Publishing Group, Westport, CT, **2007.**

[3] Jose M. Campos-Martin, Gema Blanco-Brieva, Jose L. G. Fierro, *.Angew. Chem. Int. Ed*. **2006**, 45, 6962 – 6984.

[4] K. Kosaka, H. Yamada, K. Shishida, S. Echigo, R. A. Minear, H. Tsuno, S. Matsui, *Water Res*. **2001**, 35, 3587–3594.

[5] Robert S. Disselkamp, *Energy Fuels*. **2008**, 22, 4, 2771-2774.

[6] Sanli, A. E.; Aytac, A. *Int. J. Hydrogen Energy.* **2011**, 36, 869.

[7] Kentaro Mase, Masaki Yoneda, Yusuke Yamada & Shunichi Fukuzumi. *Nature Communications*, **2016**, 7, Article number: 11470

[8] Hydrogen Peroxide Market Size By End-User (Paper & Pulp, Chemical, Waste Water Treatment, Mining), Industry Analysis Report, Regional Outlook (U.S., Canada, Germany, UK, France, Spain, Italy, China, India, Japan, Australia, Indonesia, Malaysia, Brazil, Mexico, South Africa, GCC), Application Growth Potential, Price Trends, Competitive Market Share & Forecast, 2016 – 2024

[9] Hydrogen Peroxide (HP): 2019 World Market Outlook and Forecast up to 2028

[10] G. Goor, W. Kunkel, O. Weiberg in UllmannCs Encyclopedia of Industrial Chemistry, Vol. A13 (Eds.: B. Elvers, S. Hawkins, M. Ravenscroft, G. Schulz), VCH, Weinheim, **1989**, pp. 443 – 466

[11] Jose M. Campos-Martin, Gema Blanco-Brieva, Jose L. G. Fierro. *Angew. Chem. Int. Ed*. **2006**, 45, 6962 – 6984

[12] L. W. Gosser (E.I. Du Pont de Nemours and Company), EP 132294, **1985** [Chem. Abstr. **1985**, 102, 134404].

[13] Johnson Matthey Inspiring science, enhancing life. Price tables, Johnson Matthey Base Price in US$ per troy oz, March **2019**. http://www.platinum.matthey.com/prices/price-tables#

[14] Jennifer K. Edwards, Benjamin Solsona, Edwin Ntainjua N Albert F. Carley, Andrew A. Herzing, Christopher J. Kiely, Graham J. Hutchings. *Science*. 20 Feb **2009:** Vol. 323, Issue 5917, pp.

1037-1041

[15] Li, R. *Chin. J. Catal.* **2017**, *38*, 5–12.

[16] Basic Research Needs for Solar Energy Utilization; Lewis, N. S., Crabtree, G., Eds.; Office of Science, U. S. Department of Energy: Washington, DC, **2005**.

[17] Shubin Yang, Yongji Gong, Jinshui Zhang, Liang Zhan, Lulu Ma, Zheyu Fang, Robert Vajtai, Xinchen Wang, Pulickel M. Ajayan. *Adv.Mater*.**2013**, 25, 2452–2456

[18] Xuewen Wang, Gang Liu, Zhi-Gang Chen, Feng Li, Lianzhou Wang, Gao Qing Lu and Hui-Ming Cheng. *Chem. Commun.,* **2009**, 3452-3454

[19] Zhi-An Lan, Yuanxing Fang, Yongfan Zhang, Xinchen Wang. *Angew.Chem.Int.Ed*.**2018**, 57, 470 -474

[20] Lei Wang, Yangyang Wan, Yanjun Ding, Yuchen Niu, Yujie Xiong, Xiaojun Wu and Hangxun Xu. *Nanoscale*, **2017**, 9, 4090–4096

[21] Babak Adeli and Fariborz Taghipour. *ECS Journal of Solid State Science and Technology*, **2013**, 2 (7) Q118-Q126

[22] James L. White, Maor F. Baruch, James E. Pander, Yuan Hu, Ivy C. Fortmeyer, James Eujin Park, Tao Zhang, Kuo Liao, Jing Gu, Yong Yan, Travis W. Shaw, Esta Abelev, Andrew B. Bocarsly. *Chem. Rev*.**2015**, 115, 23, 12888-12935

[23] Hiroaki Hirakawa, Masaki Hashimoto, Yasuhiro Shiraishi, and Takayuki Hirai. *J. Am. Chem. Soc.* **2017**, 139, 31, 10929-10936

[24] Longhui Zheng, Hanrui Su, Jingzhen Zhang, Laxman S. Walekar, Hamed Vafaei Molamahmood, Baoxue Zhou, Mingce Long, Yun Hang Hu. *Applied Catalysis B: Environmental* 239 (**2018**) 475–484

2. Solar Light Assisted Reductive Hydrogen Peroxide Production by polymer/TiO_2 Heterojunction Photocatalyst from Dioxygen and Water

2.1. Introduction

2.1.1. Titanium oxide

Titanium oxide (TiO_2) is a material that has many commercial applications. It is used in paints, toothpaste and sun-creams. It is also used for self-cleaning, sterilization, anti-fogging and lithography [1]. Furthermore, among the many semiconductors, TiO_2 has been used as one of the representative photocatalysts from the time when Fujishima and Honda succeeded to generate hydrogen gas and oxygen gas by splitting water with TiO_2 and Pt [2]. In addition to chemically and physically stable properties of TiO_2, other benefits, for example, low toxicity, inexpensiveness, ease to available and, proper bandgap for water splitting are mentioned as great advantages for TiO_2 to be used as a photocatalyst [3]. Despite these benefits, its large band gap and fast electron-hole recombination decrease photocatalytic productivity. The band gap of TiO_2 is known as 3.23 eV for the indirect band gap of anatase and, 3.06 eV for the direct band gap and 3.10 eV for the indirect band gap of rutile phase [4]. The visible light region is restricted to be absorbed to TiO_2 by broad band gap of it and only ultraviolet (UV) region is absorbed [5]. Because the UV is a minor portion of the solar spectrum (8% of the radiated energy to Earth's atmosphere from the Sun) and visible light occupies around 50% of solar radiation [6], the photocatalyst which cannot use visible light shows low photoactivity. To increase the photoactivity or decrease the band gap of TiO_2, many strategies were carried out by a lot of researchers. For example, doping an impurity was conducted to make new energy level between the conduction band (CB) and valence band (VB) [7]. Other methods such as surface modification [8], dye sensitization [9] and heterojunction [10] are common efforts for enhancing the efficiency of TiO_2.

2.1.2. Organic polymers as a photocatalyst

The majority of the photocatalysts are inorganic semiconductors like inorganic metal oxides, (oxy) sulfides, and (oxy) nitrides containing d^0 and d^{10} metal cation configurations [11, 12] and these have been shown high photocatalytic activities until now. However, Inorganic semiconductors are usually toxic to both the environment and human and, some of them are scarce on the Earth. On the contrary, organic semiconductors show relatively lower photo-activities than that of inorganics due to

its strong exciton binding energy [13]. Nevertheless, non-metal property, tunable optical gaps, and material abundance are advantages of organic photocatalysts [14]. In this study, PFBT which is an abbreviation for poly (fluorene-benzothiadiazole) and PFBT-derived polymers were used with TiO_2 to generate H_2O_2 under visible light. The PFBT is one kind of donor-acceptor organic conjugated polymers featuring thermal stability, tunable electronic property and chemical structure by modifying polymeric monomer [15]. The PFBT belongs to polyfluorene family polymers (PFs) featuring visible light response, high stability, and electron-hole mobility, low LUMO levels [16].

2.1.3. Heterojunction

The heterojunction is a technique used to improve photocatalytic activity. Two semiconductors which have different band gap size and positions are contacted each other. The different band gaps help to absorb a different range of solar radiation and result in enhanced light absorbance. Electrons tend to move to lower energy level and holes tend to migrate to higher energy level so, the heterojunction which aligns two differently-positioned band gaps of semiconductors makes electrons and holes separate easily and reduce recombination [17]. In general, three types of heterojunctions of the two semiconductors are possible [18].

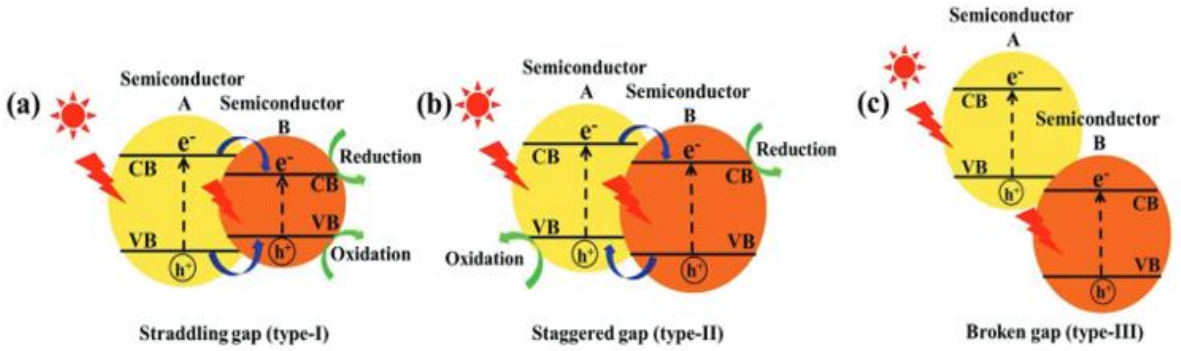

Figure 2.1. Schematic illustration of the three different types of heterojunction photocatalysts: a) type-I, b) type-II, and c) type-III heterojunctions [18].

In case of the type-I, CB of semiconductor A is higher than that of semiconductor B and VB of semiconductor A is lower than that of semiconductor B. This structure makes both electrons and holes be accumulated on the semiconductor B and separation of them isn't effective. For the type-II, both CB and VB of semiconductor A is higher than that of semiconductor B. This structure makes electrons migrate to lower CB level of semiconductor B and, holes move to higher VB level of semiconductor A, resulting in efficient separation of electron-hole pairs and reduced recombination. In

case of the type-III, even VB of semiconductor A is located on higher energy level than CB of semiconductor B so, there is no overlapped region between two band gaps. The separation of electron-hole pairs can't occur in this structure. Therefore, the type-II heterojunction is the most suitable structure for improving photoactivity.

Herein, we reported type-II of heterojunction of organic polymers with inorganic TiO_2 to produce H_2O_2 from saturated O_2 in deionized water under visible light irradiation even without a sacrificial agent.

2.2. Experimental

2.2.1. Fabrication of polymer/TiO_2 heterojunction

The 0.05 g of TiO_2 powder (Degussa, P-25) was mixed with 5wt% of three different kinds of polymers (PFBT, PFFBT and, PF2FBT) respectively and 50 mL of chloroform ($CHCl_3$, anhydrous, ≥99%, Sigma-Aldrich) was added to the mixed powder. The solution is heated and the liquid chloroform was evaporated at 70°C on the hot plate with continuous stirring. After finishing evaporation, remaining polymer/TiO_2 powder was dried overnight at room temperature and collected to test its photoactivity for production of hydrogen peroxide. These three polymers were provided by Prof. Yang's lab.

2.2.2. Characterization of polymer/TiO_2 heterojunction

Crystalline structures of the bare TiO_2, polymers, and polymer/TiO_2 were investigated by X-ray diffraction (XRD, X-per PRO, PANaloytical, Netherlands). Morphology and element analysis of the bare TiO_2 and polymer/TiO_2 were taken by scanning electron microscope (SEM, Nova Nano 230 FE-SEM), High-resolution Transmission electron microscopy (HR-TEM, JEM-2100F) and Energy-dispersive X-ray spectroscopy (EDS) mapping also done by the same instrument. To analyze the interaction between water and polymer/TiO_2 composites, and between hydrogen peroxide and polymer/TiO_2 composites, contact angle was measured by contact angle analyzer (Phoenix 300).

2.2.3. Theoretical studies

DFT calculations were carried out by the Gaussian 09 package with the nonlocal hybrid Becke three-parameter Lee–Yang–Parr (B3LYP) function and the 6-31G* basis set to elucidate the highest occupied molecular orbital (HOMO) and LUMO levels after optimizing the geometry of polymers using the same method. UV-vis-NIR absorption spectra of PFBT, PFFBT and PF2FBT and UV-vis-NIR absorption spectra of bare TiO_2 and polymer/TiO_2 heterojunction composites were recorded by UV-1800 (SHIMADZU) spectrophotometer and the Photoluminescence spectra (PL) of TiO_2, polymers, and polymer/TiO_2 were measured using a Varian Cary Eclipse fluorescence spectrometer.

2.2.4. Photocatalytic performance evaluation

Photocatalytic production of H_2O_2 by bare TiO_2 and polymer/TiO_2 heterojunction powder.

Photocatalytic activity of bare TiO2 and three polymer/TiO_2 heterojunction samples to produce hydrogen peroxide were evaluated at room temperature and pressure. 0.025g of polymer/TiO_2 heterojunction powder was dispersed in 25 mL of deionized water solution in absence of any sacrificial agent such as 2-propanol or ethanol. The colloidal solution in the reactor was purged with oxygen gas for half an hour to saturate the oxygen in the dark condition. The performance test of the H_2O_2 production was carried out with 300W Xenon lamp with continuous oxygen bubbling and to maintain dispersion, the solution was stirred by magnetic stirrer before and during the reaction. The heterojunction samples were tested under both visible light irradiation with 420nm cut-off filter and 1sun (100mW/cm^2) irradiation with 1 sun filter. 1 mL of sample was collected at every 30 min for 3 hours of the reaction by a syringe and filtrated by 0.45 μM PTFE syringe filter (Millex).

Photocatalytic production of H_2O_2 by a polymer.

Photocatalytic activities of the PFBT polymer itself to produce hydrogen peroxide were evaluated at room temperature and pressure. 0.00125g of polymer (the same amount of polymer of heterojunction in the previous experiment) was dispersed in 25mL of deionized water in absence of any sacrificial agent. To disperse the polymer powder, the reactor was sonicated for 30 minutes before the experiment. Oxygen gas was flown to solution for half an hour without light irradiation to saturate oxygen inside the system. The H_2O_2 production test was carried out with 300W Xenon lamp with continuous oxygen bubbling and stirring. Polymer samples were tested under the visible light condition with 420nm cut-off filter. 1 mL of sample was collected at every 5 min for 1 hour of the reaction by a syringe and filtrated by 0.45 μM PTFE syringe filter (Millex).

Photocatalytic decomposition of H_2O_2 by bare TiO_2 and polymer/TiO_2 heterojunction powder.

Hydrogen peroxide decomposition activity of bare TiO_2 is tested under 1sun (100mW/cm^2) intensity with 1 sun filter and polymer/ TiO_2 is tested under both visible light condition with 420nm cut-off filter and 1sun with 300W Xenon lamp with continuous stirring. 0.025g of bare TiO_2 or polymer/TiO_2 composite was dispersed in 25ml of 1mM H_2O_2 solution that was made by diluting hydrogen peroxide (35%, Alfa Aesar) in deionized water. To avoid H_2O_2 production from oxygen, the reactor was purged with nitrogen gas and oxygen gas was removed for 30 mins in dark before decomposition test.

Measurement of H_2O_2 concentration.

The concentration of generated H_2O_2 is measured by the DPD method. 1 mL H_2O_2 sample was collected by syringe from the reactor and it was filtrated by 0.45 μM PTFE filter (Millex) to separate H_2O_2-containing solution from polymer or polymer/TiO_2 powder. Sodium phosphate buffer was added to the properly diluted sample and then, deionized water is added. N,N,-Diethyl-p-phenylene-diamine sulfate (DPD, ≥98%, Sigma-Aldrich) solution (in 0.1 N sulfuric acid standard solution) and peroxidase (POD, horseradish, Sigma) solution (in deionized water) was used to make vivid color for measuring the absorbance of hydrogen peroxide. The concentration corresponding to its absorbance was automatically calculated by using UV-visible spectrophotometer (UV-2600, Shimazu).

2.3. Results & discussion

2.3.1. Synthesis and structural analysis of polymer/TiO_2 heterojunction photocatalyst

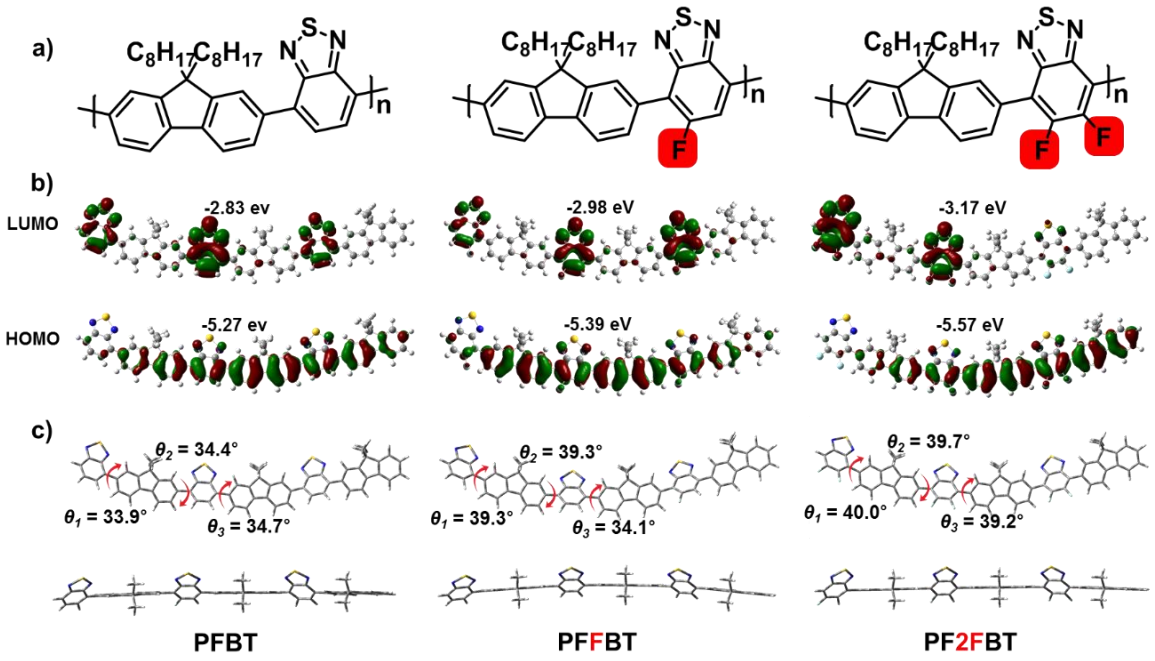

Figure 2.2. a) Molecular structures, b) simulated HOMO and LUMO orbitals of trimers, and c) calculated molecular geometries of PFBT, PFFBT, and PF2FBT polymers.

Molecular structures of polymers are shown in **Figure 2.2a.** The first polymer is poly(fluorene-benzothiadiazole) (PFBT) which is consists of a donor part (fluorene) and acceptor part (benzothiadiazole) units. Other two polymers are modified from PFBT adding fluorine atom at benzothiadiazole. The second polymer contains one more F atom it is named PFFBT. Likewise, the third polymer contains two more F atom it is named PF2FBT. Synthesis schemes and reaction conditions of these three polymers are described in **Figure 2.3**. **Figure 2.2b** and **Table 2.1** show LUMO and HOMO of the three polymers. Polymers get broader band gap (from 2.35 to 2.45 and finally to 2.57 eV) and HOMO position of the polymers steadily get deeper (from -5.90 to -6.04 and finally to -6.11 V vs. vacuum) by adding F atoms. Molecular geometries of the trimers are shown in **Figure 2.2c** and other optical properties such as the maximum wavelength of the polymers in the solution or as a thin film are described in **Table 2.2.**

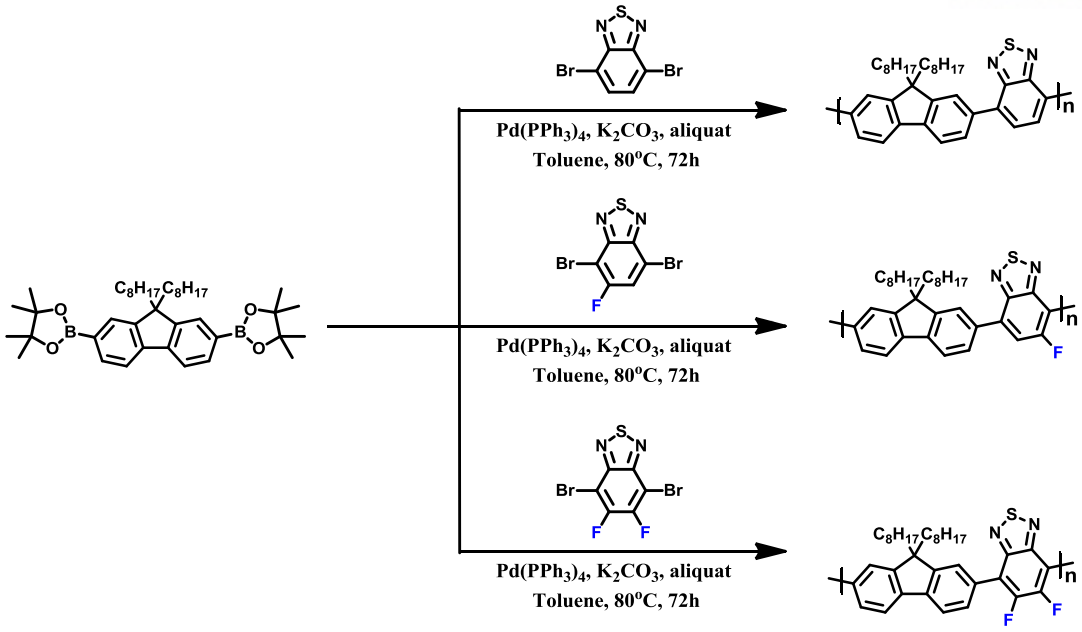

Figure 2.3. Synthetic routes to copolymers; PFBT, PFFBT, and PF2FBT

Table 2.1. Optical and electrochemical properties of polymers

	λ_{sol}^{max} [nm]	λ_{film}^{max} [nm]	λ_{onset} [nm]	E_g^{opt} [eV]	E_{HOMO} [eV]	E_{LUMO} [eV]	Mn [kDa]	PDI
PFBT	320,449	322, 466	528	2.35	-5.90	-3.55	55.4	1.5
PF1FBT	319,437	318,446	506	2.45	-6.04	-3.59	41.2	1.7
PF2FBT	319,422	320, 434	482	2.57	-6.11	-3.54	58.0	1.7

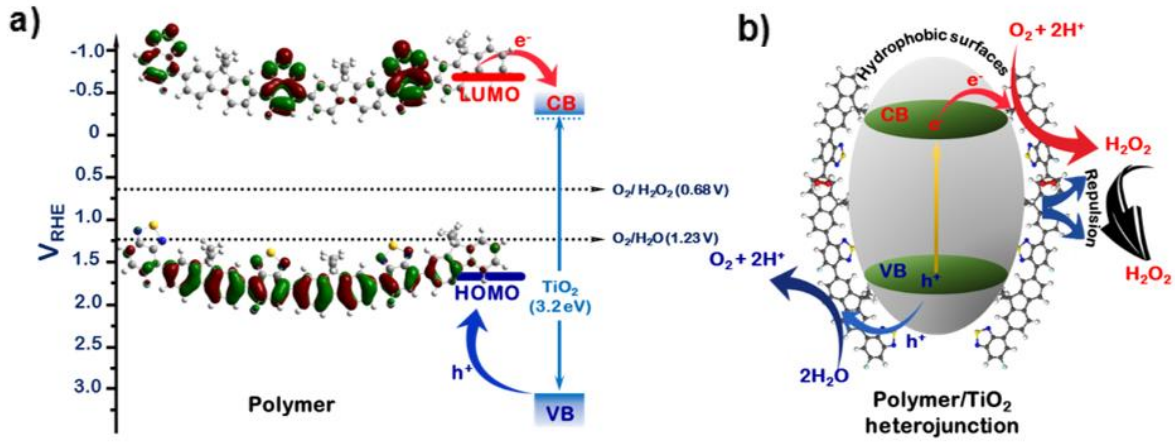

Figure 2.4. a) Schematic illustration of the charge carrier separation and transfer over fluorine modified polymer/TiO_2 composite photocatalysts with organic/inorganic heterojunction under visible-light irradiation. b) The scheme demonstrates the reductive solar H_2O_2 production from O_2 and H_2O over the polymer/TiO_2 composite where hydrophobic polymeric part not only facilitate the H_2O_2 production but also restrains the photodecomposition on the H_2O_2 over the photocatalyst surface.

The synthetic scheme of polymer/TiO_2 heterojunction photocatalyst is illustrated in **Figure 2.4b.** Organic polymers are attached on the surface of the TiO_2 and two different band gaps of the polymer and TiO_2 well construct band gap alignments that are suitable for carrier separation in **Figure 2.4a**. As already mentioned above, TiO_2 has broad band gap and both hydrogen generation potential and oxygen evolution potential is located between the conduction band and valence band of the TiO_2. Similarly, both LUMO position and HOMO position are suitable for hydrogen peroxide production for polymer because the oxygen reduction potential to hydrogen peroxide is 0.68 V and water oxidation potential to oxygen is 1.23 V. The LUMO of polymer is positioned slightly higher than the CB of TiO_2 and it indicates that photogenerated and excited electrons migrate from the LUMO of the polymer to the CB of the TiO_2. Likewise, the HOMO of the polymer is positioned much higher than the CB of TiO_2 and photogenerated and exciting holes migrate from the VB of the TiO_2 to HOMO of the polymer. This fast charge separation can reduce electron-hole recombination. Besides, the narrow band gap of the polymer (for PFBT: 2.35 eV, for PFFBT: 2.45 eV for PFFBT, and for PF2FBT: 2.57 eV in **Table 2.1**) helps polymer/TiO_2 composite to absorb the visible light range of the solar spectrum while TiO_2 itself has the broad bandgap (for anatase: 3.2 eV and for rutile: 3.0 eV) and thus, it has limitation to absorb the light except for UV regions. Enhanced charge separation due to proper band gap position and increased light absorbance due to narrow band gap of the polymer make this photocatalyst exhibit better performance to produce H_2O_2.

2.3.2. Characterization results

Morphologies of bare TiO_2, PFBT/TiO_2, PFFBT/TiO_2, and PF2FBT/TiO_2 heterojunction were observed using Nano230 FE-SEM in **figure 2.5**. The image of bare TiO_2 shows its structure and size which is around 20 nm size of particles. Compared to the other three SEM images, TiO_2 is not accumulated or aggregated thus, the smallest size of particles is observed. However, for the other three heterojunction samples, polymers have covered some parts of TiO_2. The TiO_2 particles are aggregated and form a bigger cluster. In the case of the PFBT/TiO_2 and PFFBT/TiO_2, particles are agglomerated severely and it is hard to find the boundaries between the particles. The particle size of the PFBT/TiO_2 and PFFBT/TiO_2 are hard to determine but much larger than that of bare TiO_2. Size of the PF2FBT/TiO_2 is much smaller than that of PFBT/TiO_2 and PFFBT/TiO_2 but bigger than that of bare TiO_2. Moreover, agglomerated polymers are found (red circle in **Figure 2.5**) between the particles. It indicates that the interaction between the PF2FBT itself is stronger than the other two polymers.

EDS mapping images of bare TiO_2, PFBT/TiO_2, PFFBT/TiO_2, and PF2FBT/TiO_2 heterojunction were also observed in **Figure 2.6**. Titanium and oxygen atoms were detected for pristine TiO_2 and carbon and sulfur atoms were additionally detected for polymer/TiO_2 composites. Although fluorine and nitrogen atoms were also analyzed, the error of them was too large due to low contents. For the all polymer/TiO_2 heterojunction samples, polymers were well distributed and there were no severe agglomerations. HR-TEM images of the bare TiO_2, PFBT/TiO_2, PFFBT/TiO_2, and PF2FBT/TiO_2 composites were observed in **Figure 2.7** and bare TiO_2 powders were clearly shown in **Figure 2.7a.** However, in case of other polymer/TiO_2 powders, the edge of the TiO_2 powders was not obviously shown. The polymers (the amorphous parts) are cover the particles and it makes TiO2 powders agglomerated.

XRD patterns of the pristine PFBT, PFFBT, and PF2FBT polymers are shown in **Figure 2.8a** and polymers are amorphous. XRD pattern of polymer/TiO_2 heterojunctions is compared to bare TiO_2 in **Figure 2.8b.** XRD patterns did not much change by forming a heterojunction with polymers comparing pristine TiO_2. There is no additional peak and intensity of peaks is decreased. It indicates polymers didn't invade the molecular structure of TiO_2 and only crystallinity of the polymer/TiO_2 heterojunctions is decreased due to amorphous polymers.

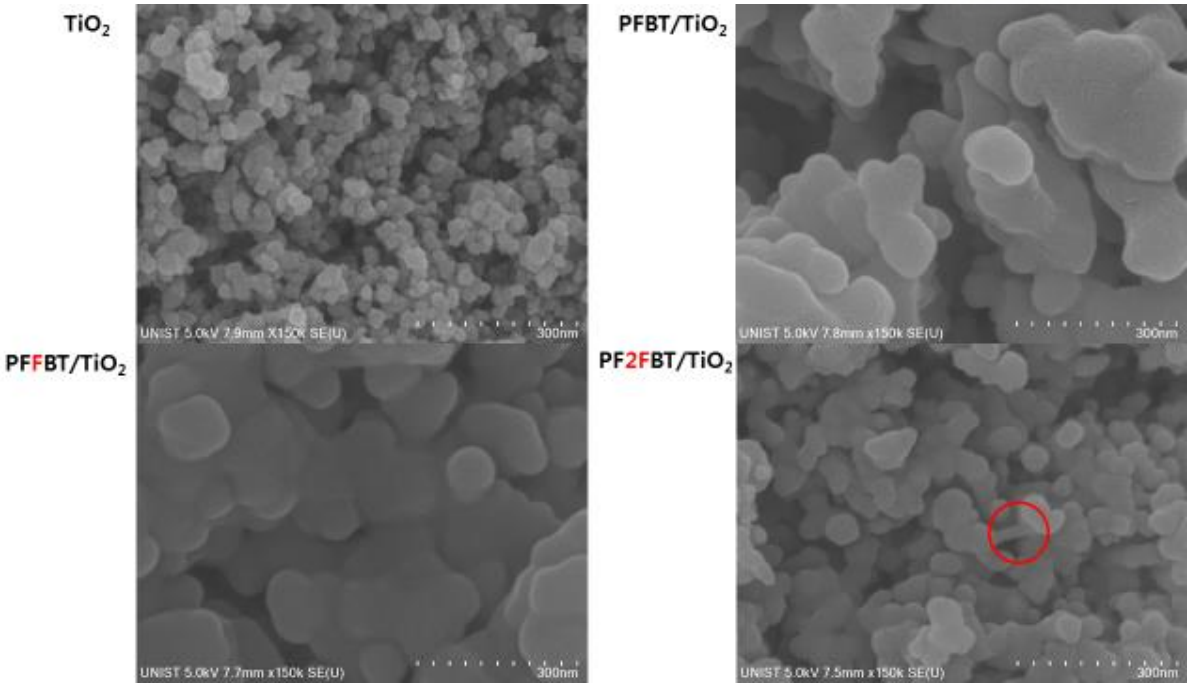

Figure 2.5. SEM images of bare TiO_2 and polymer/TiO_2 heterojunctions (PFBT/TiO_2, PFFBT/TiO_2, and PF2FBT/TiO_2).

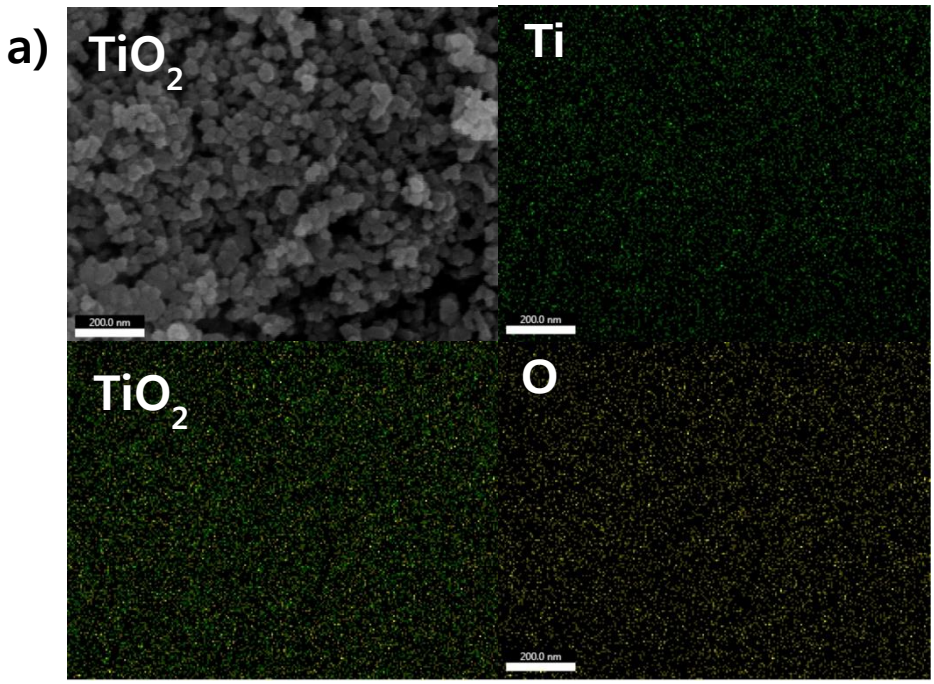

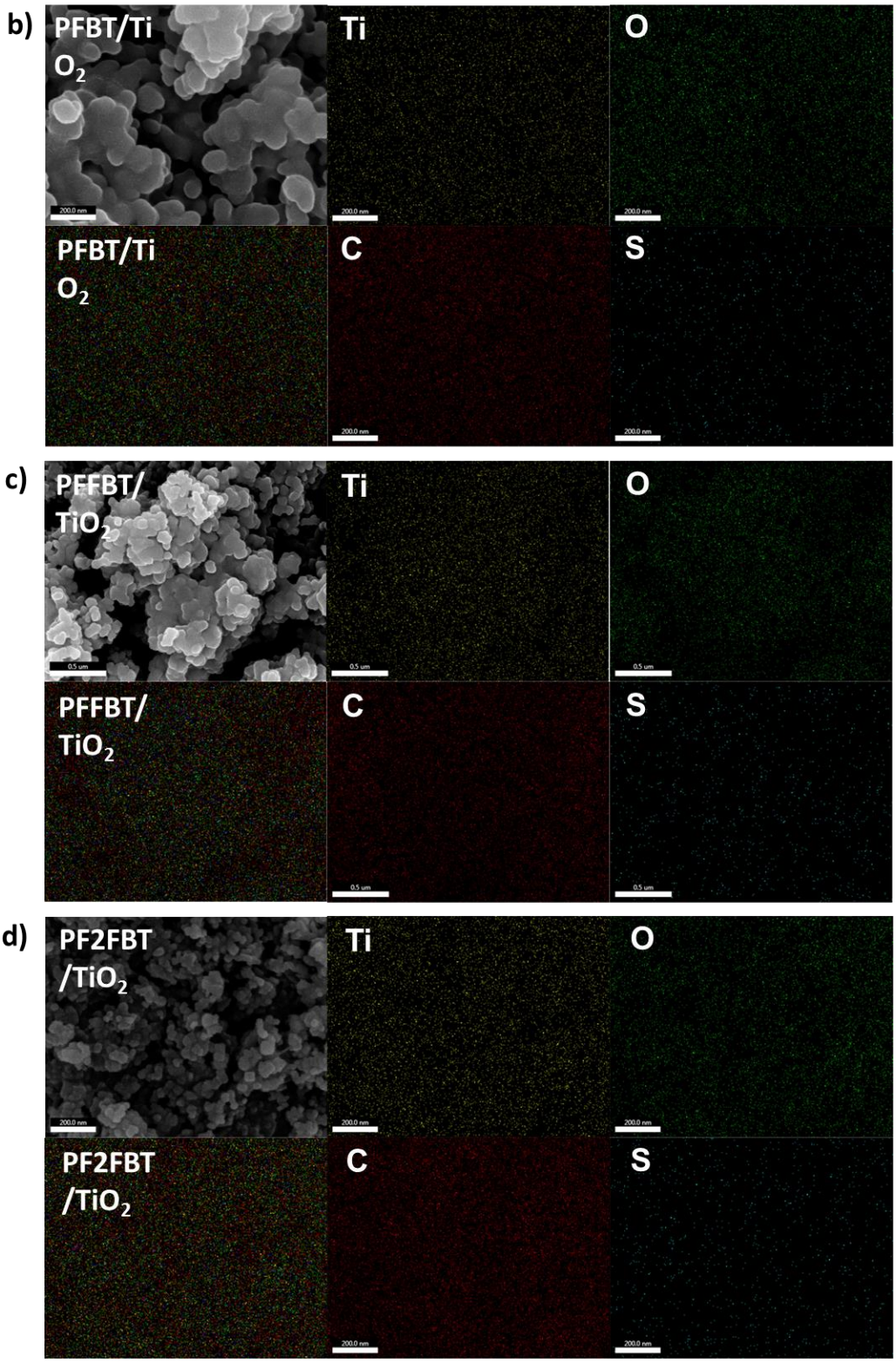

Figure 2.6. a) EDS mapping images of a) bare TiO_2 and b) PFBT/TiO_2, c) PFFBT/TiO_2, and d) PF2FBT/TiO_2

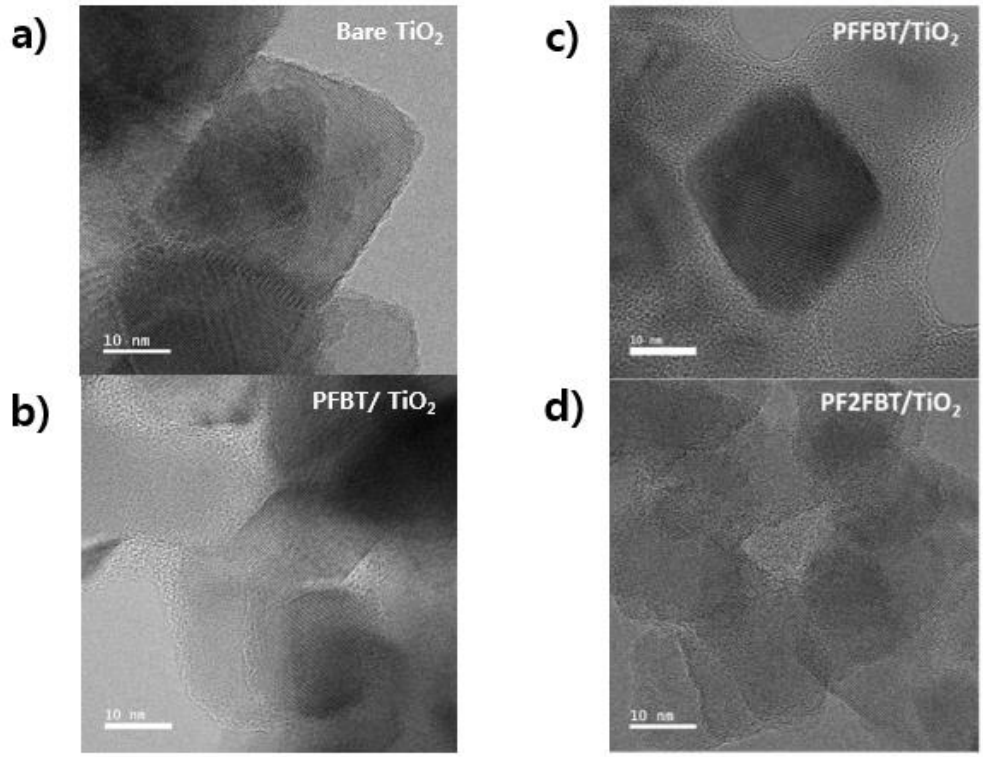

Figure 2.7. TEM images of bare TiO_2 and PFBT/TiO_2, PFFBT/TiO_2, and PF2FBT/TiO_2

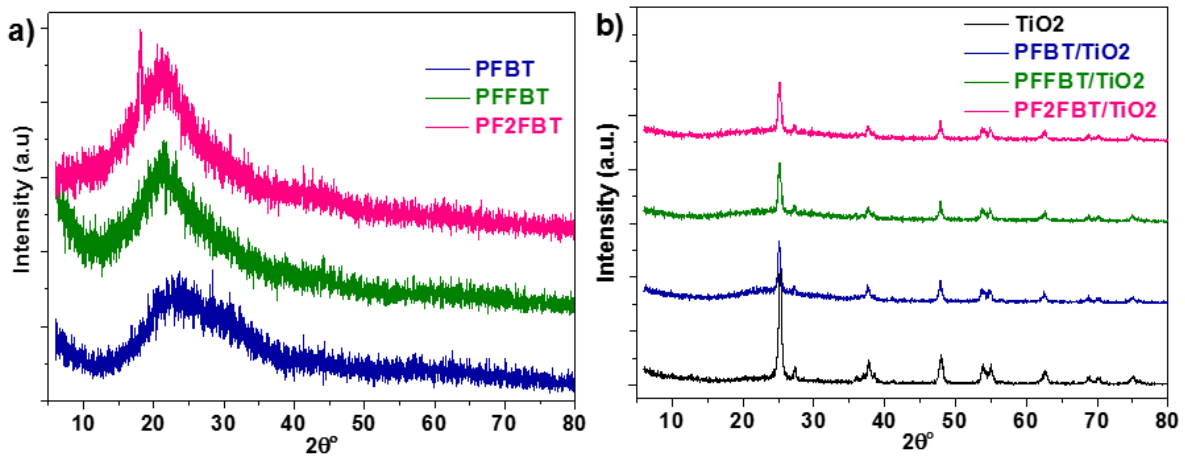

Figure 2.8. XRD patterns of a) pristine polymers (PFBT, PFFBT, and PF2FBT), and b) bare TiO_2, and polymer/TiO_2 heterojunctions (PFBT/TiO_2, PFFBT/TiO_2, and PF2FBT/TiO_2).

Absorption spectra of PFBT, PFFBT and PF2FBT in film form and solution form are shown in **Figure 2.9**. Both graphs show similar trends. The PFBT absorption spectra cover the longest wavelength region among the polymers in both cases. By adding F atoms in the polymer unit, absorption spectra shifts to a shorter wavelength region. The absorption peak of the PFFBT polymer is located slightly left side of the peak of PFBT polymer. Likewise, the absorption peak of the PF2FBT polymer is located slightly left side of the peak of PFFBT polymer. These results well match the band gap size of three polymers (for PFBT: 2.35 eV, for PFFBT: 2.45 eV for PFFBT, and for PF2FBT: 2.57 eV in **Table 2.1**) because the broader band gap can harvest a smaller range of the wavelength. Photocatalytic hydrogen peroxide production test was conducted under visible light irradiation with 420 nm cut-off filter. It means that the photons corresponding to the wavelength below 420 nm cannot be used. Thus, the PFFBT can harvest the light most compared to the other two.

Figure 2.10 shows the absorption spectra of the polymer/TiO_2 nanoparticle and pristine TiO_2. The ability to harvest light of bare TiO_2 is close to zero value over 420 nm range of wavelength. The polymer/TiO_2 heterojunctions show better absorbance. The light absorbance of PFBT/TiO_2 and PFFBT/TiO_2 are similar over the 400nm. However, the absorbance of PF2FBT/TiO_2 is much lower than that of PFFBT/TiO_2 and PFBT/TiO_2 although it is still higher than that of bare TiO_2.

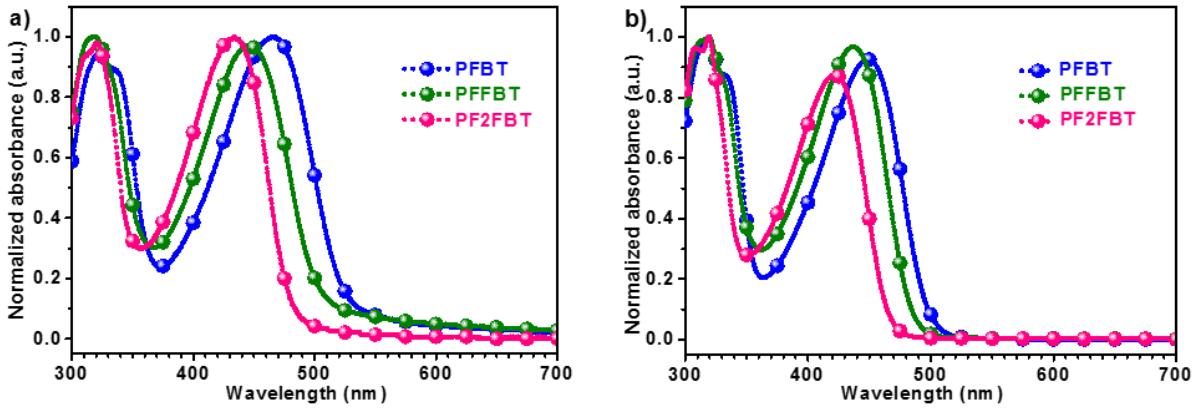

Figure 2.9. a) Normalized UV-vis-NIR absorption spectra of PFBT, PFFBT, and PF2FBT in film form, and b) polymer suspension in chloroform solution.

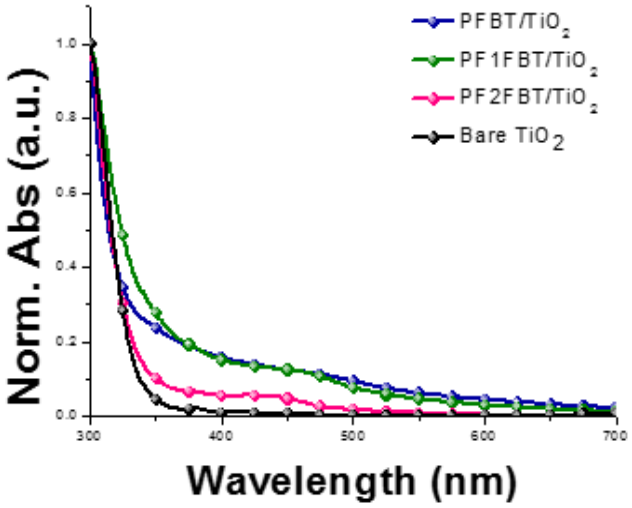

Figure 2.10. UV-vis-NIR absorption profiles of polymer/TiO_2 nanoparticle and TiO_2 films.

2.3.3. Photocatalytic activity of polymer/TiO_2

Photocatalytic activity for hydrogen peroxide production and decomposition were shown in **Figure 2.11**. **Figure 2.11a** shows a change of a concentration of H_2O_2 over time by bare TiO_2, pristine PFBT polymer, and PFBT/TiO_2 organic-inorganic heterojunction composite under visible light irradiation in absence of the sacrificial agent. The molecular structure of PFBT is described in **Figure 2.2a**. Bare TiO_2 shows negligible photoactivity in the visible light region because of the wide band gap as mentioned. PFBT polymer itself also shows low photoactivity that is almost the same as pristine TiO_2. The reason for low H_2O_2 concentration for PFBT is low dispersibility in the pure deionized water due to its hydrophobic nature. In contrast, heterojunction of polymer and TiO_2 produces a much higher concentration of H_2O_2. Its final value reaches around 45.6 μM at 3 hours later from it starts to generate H_2O_2 under visible light irradiation without any hole scavenger. Bare TiO_2 and PFBT/TiO_2 also test under 1 sunlight irradiation in the absence of hole scavenger in **Figure 2.11b**. The PFBT/TiO_2 produced about 135 μM at 3 h. Photocatalysts under 1 sun condition utilize not only visible light but also UV light irradiation and PFBT/TiO_2 composite under 1 sun recodes 3 times higher value than the concentration of H_2O_2 under visible light. In both cases, H_2O_2 production by PFBT/TiO_2 heterojunctions is much better than that of bare TiO_2 and it is firstly because of the fast

charge separation by two differently positioned band structures from polymer and TiO_2 and enhanced light absorbance by narrow band gap size of the PFBT polymer. Moreover, the hydrophobic nature of the polymer is expected as a factor for higher performance of the heterojunction sample. **Figure 2.11c** demonstrates hydrogen peroxide decomposition under 1 sunlight irradiation by TiO_2 and PFBT/TiO_2. Although the photoactivity of PFBT/TiO_2 is higher, the H_2O_2 degradation rate of TiO_2 is much faster than that of PFBT/TiO_2. The reason for slow decomposition rate of H_2O_2 by PFBT/TiO_2 heterojunction is originated from its higher hydrophobicity. Hydrogen peroxide itself acts as a hole scavenger and easily decomposed by photogenerated holes from the photocatalyst when it is adsorbed on the surface of the photocatalyst. However, the hydrophobic nature of polymer contacted on the TiO_2 surface prevent H_2O_2 onto the photocatalyst surface. Consequently, hydrogen peroxide maintains a higher concentration like **Figure 2.11c.** In this figure, only half of the H_2O_2 is degraded by polymer/TiO_2 heterojunction at 15 min while almost all the H_2O_2 is decomposed by TiO_2 at the same time. Additionally, this property of a polymer is the main reason for higher H_2O_2 generation rate in **Figure 2.11a** and **2.11b** as well as the advantages from the heterojunction (increased light absorbance and rapid charge separation).

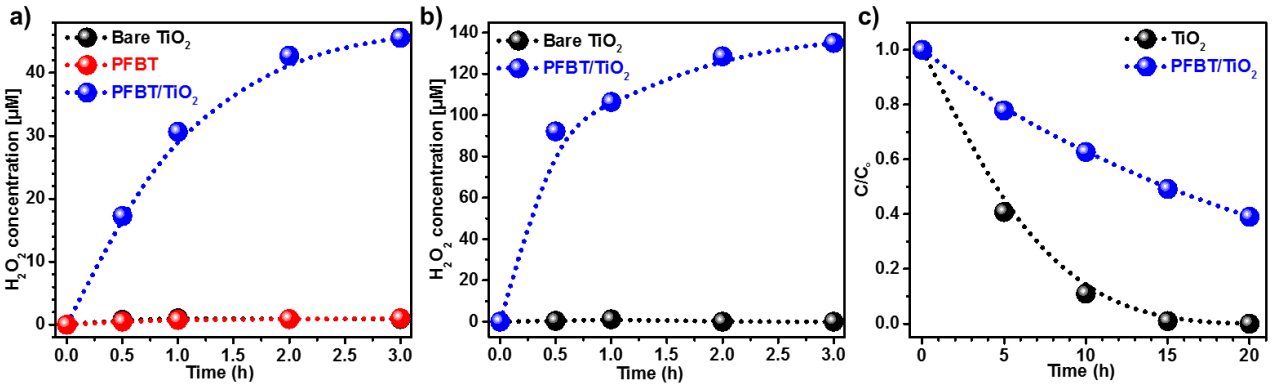

Figure 2.11. Photocatalytic hydrogen peroxide production of bare TiO_2, pristine polymer, and PFBT/TiO_2 heterojunction a) under visible light (λ > 420 nm), and b) 1 sun light (100 mW cm^{-2}) irradiation without using hole scavenger. c) Photocatalytic hydrogen peroxide decomposition of bare TiO_2 and PFBT/TiO_2 heterojunction under 1 sun light (100 mW cm^{-2}) irradiation.

To construct more efficient heterojunction photocatalyst for hydrogen peroxide production, more hydrophobic polymers named PFFBT and PF2FBTare synthesized. The molecular structure of PFFBT and PF2FBT are described in **Figure 2.2a**. Synthetic routes for three polymers PFBT, PFFBT and PF2FBT are described in **Figure 2.3**. To verify the real hydrophobicity of three polymers and three heterojunction samples, contact angles were measured on the glass with H_2O in **Figure 2.12**. The hydrophobicity can be judged according to the size of the contact angle. The most hydrophilic material is TiO_2 as expected and its contact angle is 30.1°. It is confirmed that the hydrophobicity was increased as the F-atom was doped in the polymer in **Figure 2.12a**. The contact angle of PFBT that is basic polymer before F atom doping is 91.3° and the contact angle of one fluorine atom added polymer, PFFBT, is increased to 97.0°. The largest contact angle is 100.6° by PF2FBT which contains two fluorine atoms in their unit. Hydrophilic TiO_2 also shows a significant increase in hydrophobicity after heterojunction with three different polymers, and heterojunction with the polymer containing two F-atoms makes the TiO_2 most hydrophobic in **Figure 2.12b**. Contact angles with H_2O_2 (in **Figure 2.13**) also show the same trends with contact angles with H_2O and all angles are slightly increased compared to the angles with H_2O. By adding F atoms in polymer, the attraction between the polymer and hydrogen peroxide was decreased from 97.6° to 106.8°. likewise, the composite of TiO_2 with modified polymers has less H_2O_2 attraction than bare TiO_2. This is the reason for the slow decomposition of hydrogen peroxide by PFBT/TiO_2 in **Figure 2.11c**. The TiO_2 composite with polymers that has two F atoms in their unit has the lowest attraction with H_2O_2. This data obviously indicate that H_2O_2 degradation rate will be decreased with fluorination of the polymer.

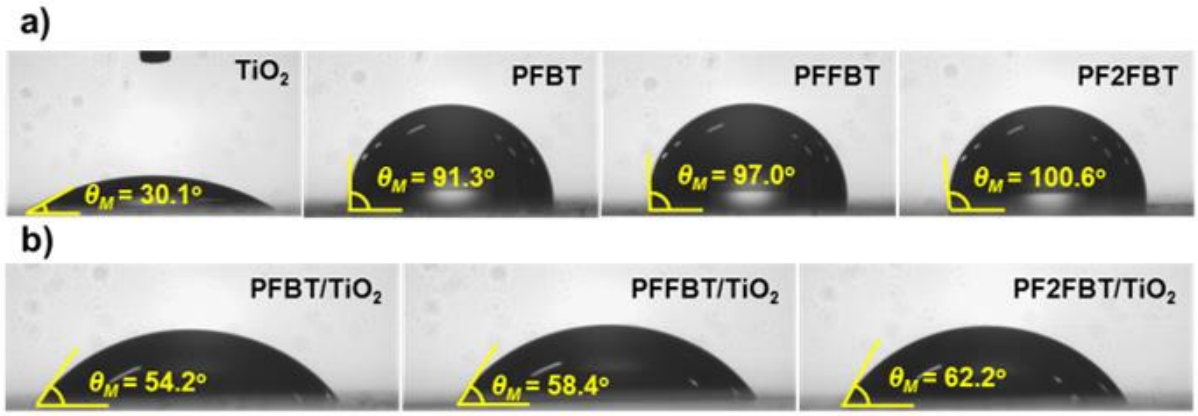

Figure 2.12. Evaluation of hydrophobicity of pristine TiO_2 polymers, and polymer/TiO_2 conjugated photocatalysts with H_2O: a) Contact angle measurement of bare TiO_2, and pristine polymers (PFBT, PFFBT, and PF2FBT), and b) polymer/TiO_2 composite films on the glass with H_2O.

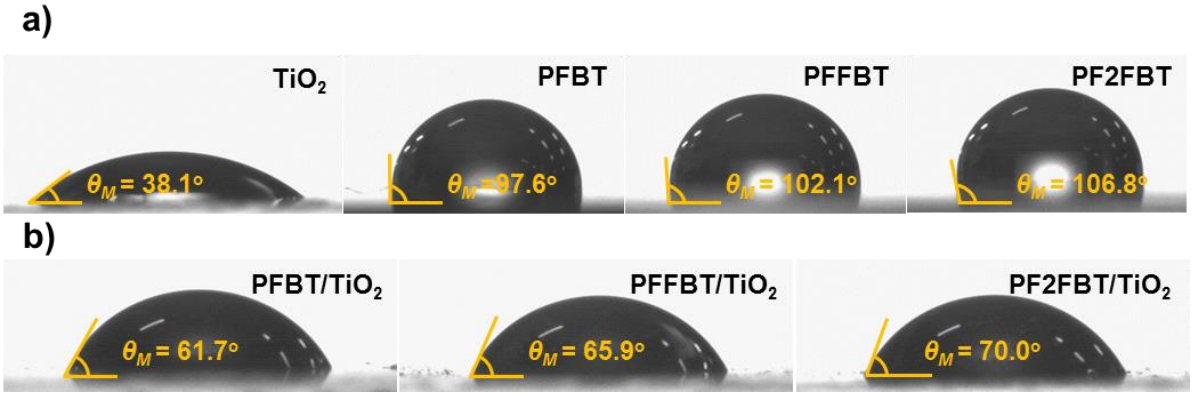

Figure 2.13 Evaluation of hydrophobicity of pristine TiO_2 polymers, and polymer/TiO_2 conjugated photocatalysts with H_2O_2: a) Contact angles of bare TiO_2 and neat copolymers films; (b) pristine polymers (PFBT, PFFBT, and PF2FBT), and b) polymer/TiO_2 composite films on the glass with H_2O_2.

PL spectra of polymers in Chloroform solution and as fabricated films in the visible region were shown in **Figure 2.14a** and **b**. In both cases, the intensity of the PL peaks among three polymers are almost same but fluorination makes the peaks shift to lower wavelengths. PL spectra of polymer/TiO_2 nanoparticles and TiO_2 in both UV and visible light region were recorded in **Figure 2.14c**. Bare TiO_2 itself is hard to activate under visible light region due to broad band gap so, its peak is close to zero value. On the other hand, three polymer/TiO_2 composite show responses. Peak intensity of PL spectra is corresponding to charge recombination and PF2FBT/TiO_2 has much higher peak intensity than the other two heterojunction samples above the 450nm wavelength range. It indicates that the recombination rate of the PF2FBT/TiO_2 is faster than that of the other two in visible light. **Figure 2.15a** demonstrates a change of a concentration of H_2O_2 over time by bare TiO_2, and three polymer/TiO_2 organic-inorganic heterojunction composites under visible light irradiation in the absence of the sacrificial agent. Bare TiO_2 didn‘t generate H_2O_2 in the visible light irradiation due to its larger bandgap but other three polymer/TiO_2 samples generated hydrogen peroxide even without a sacrificial agent. In this figure, heterojunctions of TiO_2 with one F atom-containing polymer and two F atom-containing polymer shows similar photoactivity for generating H_2O_2. The concentration of $H_2O_2$by PFFBT/TiO_2 and PF2FBT/TiO_2 is increased by 79 times compared to the concentration of it formed by bare TiO_2 although two F atom-containing a polymer has the greatest hydrophobicity and is proper to prevent the degradation of H_2O_2. The reason for similar photoactivity of two composites

is originated from the band gap (in **Table 2.1**) and recombination rate (in **Figure 2.14c**). The broader band gap of PF2FBT limits the longer wavelength in the visible light to be harvested and rapid recombination rate of the PF2FBT/TiO_2 reduces its photoactivity under visible light irradiation. Hydrogen peroxide degradation by bare TiO_2, and three polymer/TiO_2 heterojunction composites over time under 1 sunlight is shown in **Figure 2.15b**. Without photocatalysts, 1mM of H_2O_2 didn't decompose by light. In contrast, TiO_2 decomposed 1 mM of H_2O_2 to zero within 15 min. In the case of PFFBT/TiO_2, 50 % of H_2O_2 still remained at 15 min as already mentioned. The ability to prevent H_2O_2 decomposition is higher for PFFBT/TiO_2, and PF2FBT/TiO_2 heterojunctions. In both cases, more than 80 % of H_2O_2 remained at 15 min and PF2FBT/TiO_2 inhibited adsorption of H_2O_2 on the surface of it slightly well comparing PF2FBT/TiO_2 at the end because of the highest hydrophobic property.

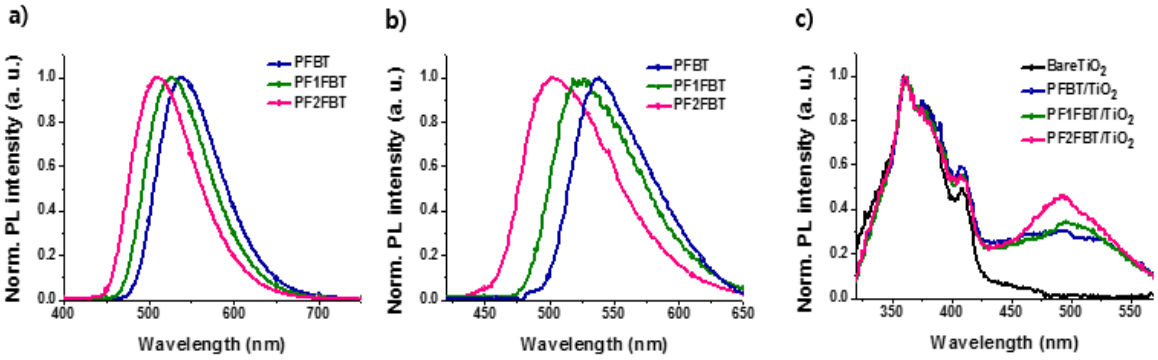

Figure 2.14. a) Photoluminescence spectra (PL) of polymers in Chloroform solution, excited at 390 nm, b) fabricated into a film, excited at 410 nm and c) Photoluminescence spectra (PL) of polymer/TiO_2 nanoparticle and TiO_2 films, excited at 310 nm.

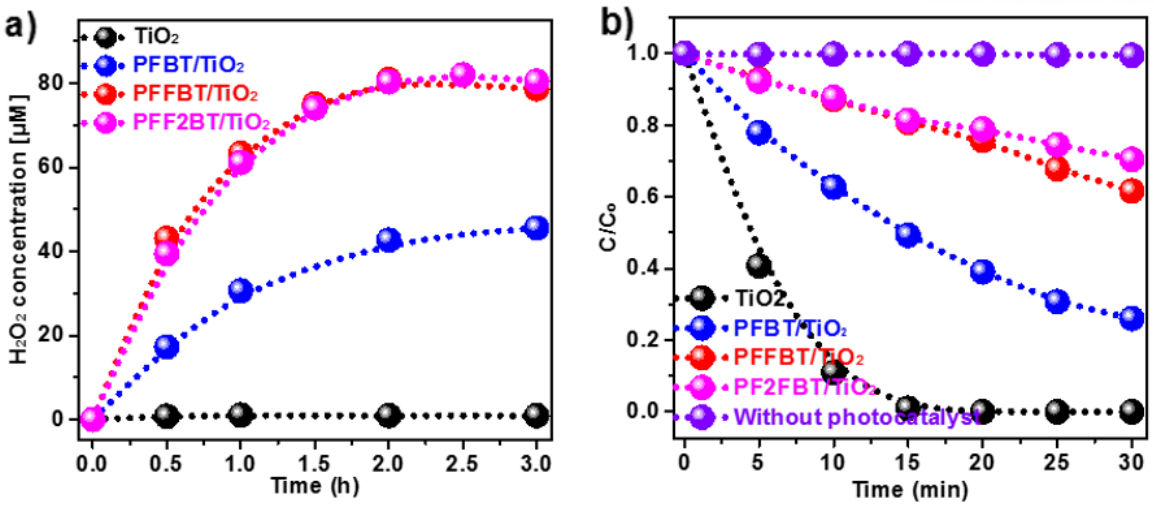

Figure 2.15. a) Comparison of photocatalytic H_2O_2 production over bare TiO_2, PFBT/TiO_2, PFFBT/TiO_2, and PF2FBT/TiO_2 heterojunction under visible light ($\lambda > 420$ nm) irradiation without using hole scavenger, and b) Photocatalytic H_2O_2 decomposition over bare TiO_2, PFBT/TiO_2, PFFBT/TiO_2, and PF2FBT/TiO_2 heterojunction under 1 sun light (100 mW cm^{-2}) irradiation.

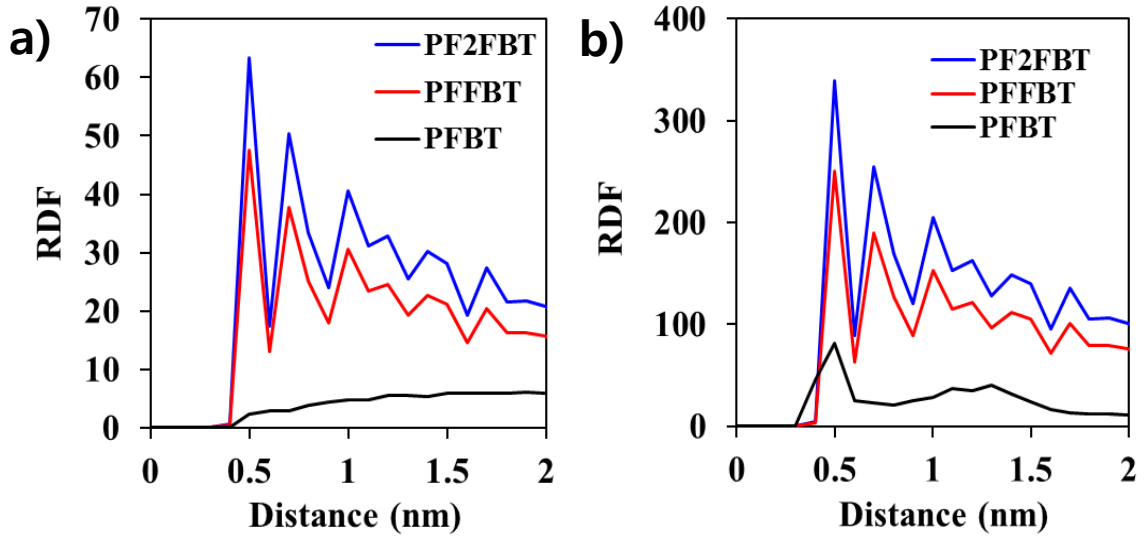

Figure 2.16. RDF v.s. distance of each polymers. a) Interaction between benzothiadiazole in polymer and TiO_2 nanoparticles, b) Interaction between benzothiadiazoles in polymers.

a)

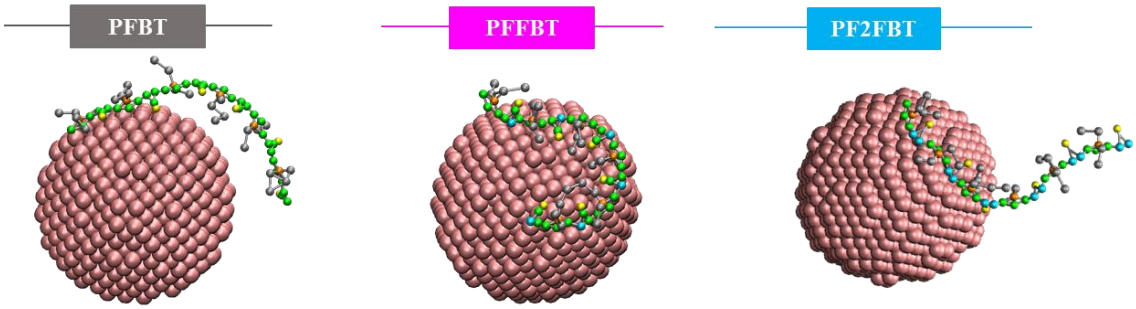

b)

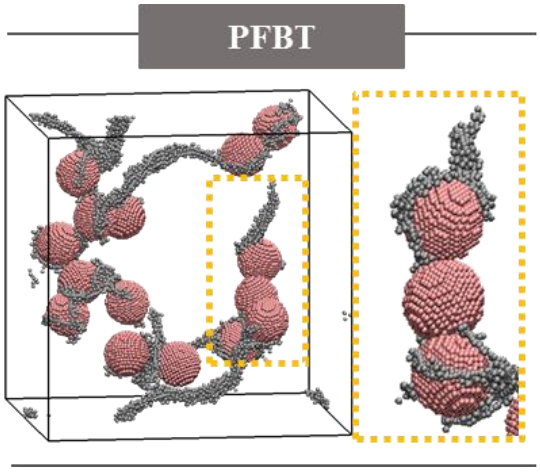

c)

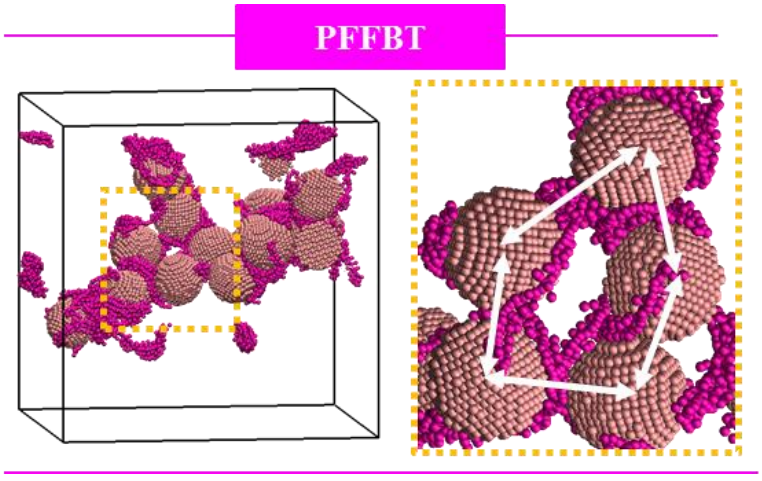

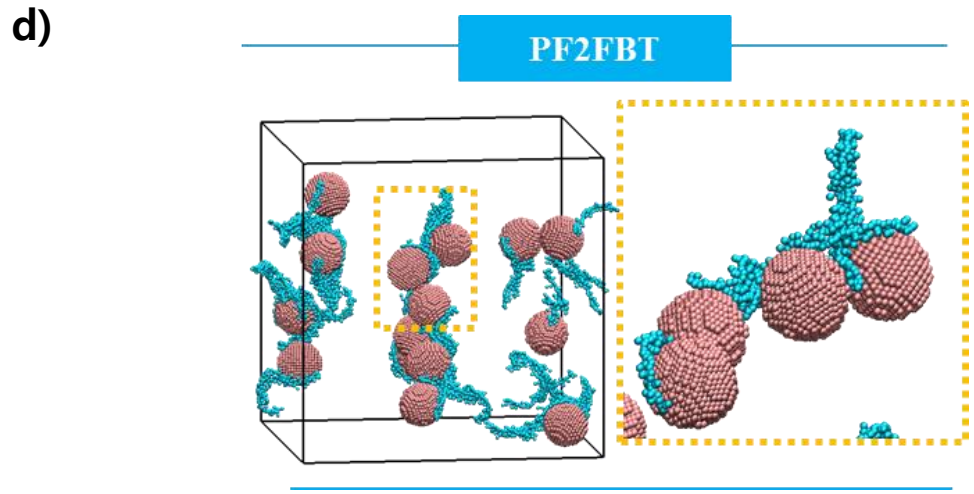

Figure 2.17. Simulation study for molphology of a) PFBT/TiO_2, PFFBT/TiO_2, PF2FBT/TiO_2 heterojunction powders respectively , b) PFBT/TiO_2 heterojunction powders inside a water system, c) PFFBT/TiO_2 heterojunction powders inside a water system, d) PF2FBT/TiO_2 heterojunction powders inside a water system.

Simulation study was carried out in **Figure 2.16 and 2.17**. **Figure 2.16a** shows the adsorption between benzothiadiazole units in the three polymers and TiO_2 nanoparticles. The interaction increased with fluorination so PF2FBT highly interact with titanume dioxide nanoparticles. **Figure 2.16b** shows the adsorption between benzothiadiazoles in polymers. Likewise, interaction between polymers increased with fluorination. However, compared to the interaction of the polymer-TiO_2, that of the polymer-polymer was too strong in case of PF2FBT. Thus, PFFBT polymers can easily aggregated with themselves and agglomeration of polymer was observed in SEM images and simulation data in **Figure 2.17d**. The best interaction and adsorption of polymer over the surface of the TiO_2 was observed in PFFBT/TiO_2 heterojunction in **Figure 2.17a**. Besides, simulations in **Figure 2.17b** and **d** show that the PFBT and PF2FBT cover low surface area over the TiO_2 nanoparticles in multi-TiO_2 powder system in the pure water and the best coverage of polymer is shown in PFFBT/TiO_2 in **Figure 2.17c**.

2.4. Conclusion

In summary, polymer/TiO_2 heterojunction is an efficient photocatalyst for hydrogen peroxide production without the addition of sacrificial agent. It shows higher hydrogen peroxide production and by preventing photodecomposition of photogenerated H_2O_2. By constructing polymer heterojunction with TiO_2, it achieved three advantages. i) Titanium dioxide can have photoactivity under visible light while it cannot react due to its large bandgap. ii) Heterojunction makes photo-induced charge carriers separated fast and reduces electron-hole recombination. iii) Hydrophobic polymer on the surface of the photocatalyst prevents hydrogen peroxide to approach to photocatalyst and adsorb on the surface of it and degradation rate of hydrogen peroxide is much slower than that of bare TiO_2. Polymer modification by fluorination for improving hydrophobicity was well applied to produce a higher concentration of H_2O_2. The measurements of the contact angles proved the increase of hydrophobicity by fluorination. Two modified polymers with TiO_2 heterojunction generates much more concentration of hydrogen peroxide and decomposed less amount of it. Because of the high recombination of electron-hole pairs, larger band gap of PF2FBT, and agglomeration of PF2FBT in multiple-TiO_2 particles system in pure water condition, PF2FBT/TiO_2 has similar activity with PFFBT/TiO_2 while it features the highest hydrophobicity among the polymer/TiO_2 heterojunctions.

2.5. References

[1] Materials Science in Semiconductor Processing. Volume 42, Part 1, February **2016**, Pages 2-14

[2] Fujishima A, Honda K. Nature. **1972** Jul 7; 238(5358):37-8.

[3] Yoshihisa Ohko, Kazuhito Hashimoto, and Akira Fujishima. J. Phys. Chem. A **1997**, 101, 43, 8057-8062

[4] Andrea Welte, Christoph Waldauf, Christoph Brabec, Peter J.Wellmann. Volume 516, Issue 20, 30 August **2008**, Pages 7256-7259

[5] Swagata Banerjee, Suresh C. Pillai, Polycarpos Falaras, Kevin E. O'Shea, John A. Byrne, and Dionysios D. Dionysiou. J. Phys. Chem. Lett. **2014**, 5, 2543−2554

[6] Moan, Johan Emilian. *7 Visible Light and UV Radiation*, **2004**.

[7] Pallabi Goswami and Jatindra Nath Ganguli. Dalton Trans., **2013**, 42, 14480

[8] Michael Nolan. *Chem. Commun*., **2011**, 47, 8617–8619

[9] Lun Pan, Ji-Jun Zou*, Xiangwen Zhang, and Li Wang. *J. Am. Chem. Soc*. **2011**, 133, 26, 10000-10002

[10] Rachel Fagan, Declan E. McCormack, Steven J. Hinder and Suresh C. Pillai. *Materials*, **2016**, 9, 286

[11] Guigang Zhang, Zhi-An Lan, and Xinchen Wang. *Angew. Chem. Int. Ed.* **2016**, 55, 15712 – 15727

[12] Xiaobo Chen, Shaohua Shen, Liejin Guo, and Samuel S. Mao. *Chem. Rev.* **2010**, 110, 6503–6570

[13] Yu-Wei Su, Wei-Hao Lin, Yung-Jung Hsu, and Kung-Hwa Wei. *Small*, **2014**, 10, No. 22, 4427–4442

[14] Lei Wang, Ricardo Fernández-Terán, Lei Zhang, Daniel L. A. Fernandes, Lei Tian, Hong Chen, Haining Tian. *Angew. Chem. Int. Ed*. **2016**, 55, 12306–12310

[15] Fengtao Yu, Zhiqiang Wang, Shicong Zhang, Haonan Ye, Kangyi Kong, Xueqing Gong, Jianli Hua, He Tian. *Adv. Funct. Mater,* **2018**, 28, 1804512

[16] Jie Chen, Chung-Li Dong, Daming Zhao, Yu-Cheng Huang, Xixi Wang, Leith Samad, Lianna

Dang, Melinda Shearer, Shaohua Shen, Liejin Guo. *Adv.Mater.***2017**, 29, 1606198

[17] Huanli Wang, Lisha Zhang, Zhigang Chen, Junqing Hu, Shijie Li, Zhaohui Wang, Jianshe Liu and Xinchen Wang. *Chem. Soc. Rev.*, **2014**, 43, 5234

[18] Jingxiang Low, Jiaguo Yu, Mietek Jaroniec, Swelm Wageh, Ahmed A. Al-Ghamdi *Adv.Mater*. **2017**, 29, 1601694

3. Solar Light Assisted Reductive Hydrogen Peroxide Production by MOF-Derived Carbon@CdS Photocatalyst from Dioxygen and Water

3.1. Introduction

3.1.1. Cadmium sulfide

Many photocatalysts such as TiO_2, ZnO, ZrO_2, and ZnS have broad band gap over 3.0eV and these large ranges of band gap prevent visible light to be absorbed to photocatalysts. However, cadmium sulfide (CdS) is semiconductor that has narrow band gap estimated to be 2.42 eV and it is suitable photocatalyst to split water because its conduction band is above the H^+/H_2 redox potential and its valence band is below the O_2/H_2O redox potential [1]. After Darwent and Porter succeeded reduction of H_2O to H_2 using CdS under visible light irradiation first in 1981 [2], CdS have been used as a photocatalyst but, it has several disadvantages. First, it has unstable photochemical properties. Second, the photogenerated electron-hole pair recombination is fast [3]. Third, because of the oxidation by the photogenerated hole, it degrades itself and results in serious photocorrosion problem [4]. To overcome these problems, many researchers have set strategies. For example, core-shell structured Ni_2P@CdS was synthesized to resist to CdS photocorrosion property. The Ni_2P shell on the surface of CdS prevents CdS photocorrosion [5]. Also, other researches such as surface modification of CdS by conjugated derivatives from polyvinyl chloride [6], ultrathin yet highly impermeable graphene layers-draped CdS [7] and, construction of CdS/NixSy@NF heterostructure [8] were done for anti-photocorrosion of CdS and improved visible-light photoactivity.

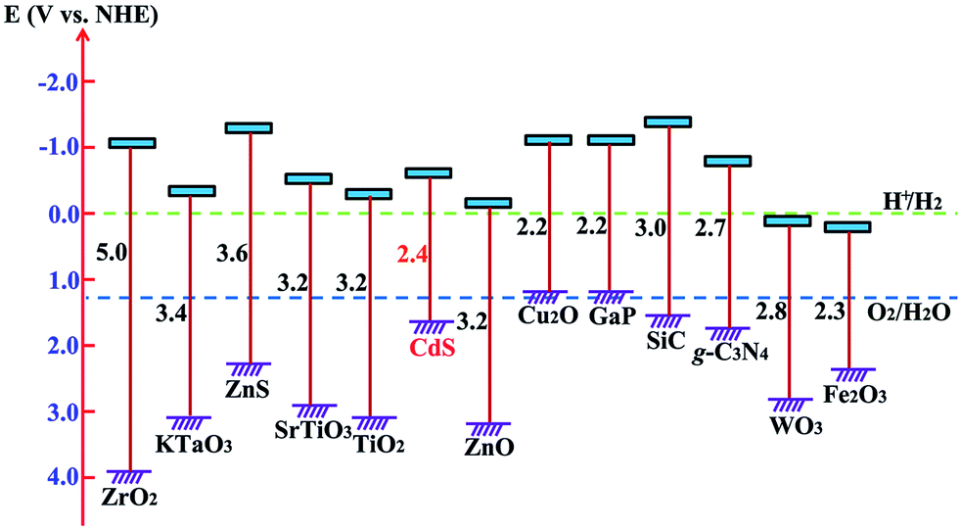

Figure 3.1. Band gap energy and VB and CB positions for a range of semiconductors [1].

3.1.2. MOF structure

Metal-organic frameworks (MOFs) consists of metal ions or clusters and organic linkers and has porous and crystalline characteristics [9]. Because it features high surface area and tunable pore volumes, it is applied to various field. For example, gas storage, gas separation, drug delivery, and proton-conductivity [10]. MOF also considered as potential candidates for photocatalytic reactions [11]. Zhang *et al* used MIL–53(Fe) hybrid magnetic composites for photoelectrochemical O_2 evolution [12] and Cavka *et al* presented the zirconium-based MOF (UiO-66(Zr): $[Zr_6O_4(OH)_4(CO_2)_{12}]$) for H_2 evolution [13]. Fu *et al* introduced MOF NH_2-MIL-125(Ti) material for CO_2 reduction to $HCOO^-$ [14]. However, MOF suffers from poor thermal and chemical stability compared to other inorganic porous materials or zeolites [15]

Herein, we directly synthesized CdS photocatalyst that carbon matrix exists on the surface. Carbon is originated from an organic ligand of MOF structure and carbonization process form it during annealing of the MOF at high temperature. Because of the thermally unstable property, MOF structure transforms to crystalline CdS. The Carbon matrix on the MOF-derived CdS can slow hydrogen peroxide decomposition rate down. Hydrogen peroxide is generated by this MOF-derived carbon@CdS composite under visible light irradiation without sacrificial agent. Compared to commercialized CdS, its performance to produce H_2O_2 and to restrain the degradation of H_2O_2 were outstanding.

3.2. Experimental

3.2.1 Synthesis method

Preparation of [Cd(EDDA)]. $Cd(NO_3)_2 \cdot 4H_2O$ (1.54 g, 5 mmol) and H_2EDDA (1.05 g, 5 mmol) were dissolved in a mixture of *N*,*N*-dimethylformamide (DMF) and H_2O (100 mL, 1:1, v/v). The mixture solution was placed in a 500 mL glass reaction vessel, and heated at a rate of 1 ℃/min and maintained at 80 ℃ for 12 h. After cooling to room temperature, colorless crystals were filtered off and briefly washed with water and ethanol. Yield: ~23.5%. Anal. Calcd for $Cd_1C_6H_8O_4S_2$: C, 22.47; H, 2.51; N, 0.00; S, 20.00. Found: C, 22.47; H, 2.49; N, 0.00; S, 20.74. FT-IR (ATR, cm^{-1}): $\nu_{C\text{-}H}$ 2969, 2914 (w), $\nu_{C\text{-}O=O}$ 1566, 1370 (s). The hydrothermal reaction with a small portion of triethylamine (1.4 mL, 10 mmol) also afforded the synthesis of the same compound in powder form.

3.2.2. Characterization methods

To clarify crystalline structure of the CdEDDA that is MOF and MOF-derived carbon-encapsulated samples ($CdS_{O2,\ 6h}$, $CdS_{O2,\ 12h,}$ and $CdS_{O2,\ 24h}$), X-ray diffraction (XRD) patterns were recorded by a Bruker D2 phaser diffractometer. Thermogravimetric analysis (TGA) were performed by Q50 from TA Instruments under N_2 atmosphere with a 5 ^oC/min of a scan rate.

Morphology data and elementary analysis data were taken by transmission electron microscopy (TEM) images and energy-dispersive X-ray spectrometry (EDS) mapping by JEOL JEM-2100 microscope. Scanning electron microscopy (SEM) images were found by a Quanta 200 microscope (FEI) for morphology analysis.

3.2.3. Photocatalytic performance test

Photocatalytic production of H_2O_2 by commercial CdS and MOF-derived CdS.

Photocatalytic activity of commercial CdS and MOF-derived CdSs samples for hydrogen peroxide production were evaluated at room temperature and pressure. 0.1g of photocatalyst powder was dispersed in 100 ml of deionized water in absent of any sacrificial agent such as 2-propanol or ethanol. The colloidal solution in the reactor was purged with oxygen gas for half an hour to saturate the oxygen in the solution in the dark condition. The performance test of the H_2O_2 production was carried out with 300W Xenon lamp with continuous oxygen bubbling. To maintain dispersion, the solution was stirred by magnetic stirrer before and during the reaction. The photocatalyst samples were tested under both visible light irradiation with 420nm cut-off filter and 1sun (100mW/cm^2) irradiation with 1 sun filter. 1 mL of sample was collected at every 30 min for 3 hours of the reaction by a syringe and filtrated by 0.45 μM PTFE syringe filter (Millex).

Photocatalytic decomposition of H_2O_2 by commercial CdS and MOF-derived CdS.

Hydrogen peroxide decomposition activity of commercial CdS and MOF-derived CdS is tested under 1sun (100mW/cm^2) intensity with 1 sun filter and polymer/ TiO_2 is tested under visible light irradiation with 420nm cut-off filter with 300W Xenon lamp with continuous stirring. 0.1 g of commercial CdS and MOF-derived CdSs was dispersed in 100 ml of 1mM H_2O_2 solution that was made by diluting hydrogen peroxide (35%, Alfa Aesar) in deionized water. To avoid H_2O_2 production from oxygen, the reactor was purged with nitrogen gas and oxygen gas was removed for 30 mins in dark before decomposition test.

Measurement of H_2O_2 concentration.

The concentration of generated H_2O_2 is measured by DPD method. 1 mL H_2O_2 sample was collected by syringe from the reactor and it was filtrated by 0.45 μM PTFE filter (Millex) to separate H_2O_2-containing solution from photocatalyst powders. Sodium phosphate buffer was added to the properly diluted sample and then, deionized water is added. N,N,-Diethyl-p-phenylene-diamine sulfate (DPD, ≥98%, Sigma-Aldrich) solution (in 0.1 N sulfuric acid standard solution) and peroxidase (POD, horseradish, Sigma) solution (in deionized water) was used to make vivid color for measuring absorbance of hydrogen peroxide. The concentration corresponding its absorbance was automatically calculated by using UV-visible spectrophotometer (UV-2600, Shimazu).

3.3. Results & discussions

3.3.1. Transformation of MOF to carbon@CdS

Synthetic method of MOF structure CdEDDA is described in **Figure 3.2**. Firstly, the MOF structure CdEDDA containing cadmium and sulfur atoms were synthesized *via the* solvothermal method. Cadmium is originated from cadmium nitrate hexahydrate precursor and it is metal part of MOF structure. Sulfur is originated from ethylenedithiodiacetic acid that acts as an organic ligand in MOF structure. Then, CdEDDA is thermally treated again to be synthesized as a photocatalyst. This procedure is demonstrated in **Figure 3.3**. The CdEDDA was annealed for different time intervals under oxygen atmosphere to form CdS photocatalyst directly from MOF structure. CdEDDA annealed 0h means untreated sample so, it still has a MOF structure. In the case of three hours of annealing of CdEDDA, MOF structure remains and no CdS is formed yet. However, in case of over six hours of annealing, the MOF structure is fully-destructed by a long time of heating at high temperature. The organic ligand of the MOF is carbonized and form carbon matrix on the surface of the CdS. It is expected that the stability of the CdS is enhanced by the formation of the carbonized organic ligands on its surface and is reduced the decomposition rate of the generated H_2O_2. Moreover, mobility and ability to the separation of the carriers are also improved by the carbon matrix on the surface of the photocatalyst. **Figure 3.4** described both bare CdS and as-synthesized CdS which has carbonized-MOF on its surface. Carbon matrix on the CdS photocatalysts well blocks the approach of the photogenerated H_2O_2. Because the adsorption of the H_2O_2 to the surface of the photocatalyst is well prevented due to the carbonized layer on the CdS, produced H_2O_2 can be avoidable to be decomposed. Thus, the concentration of the hydrogen peroxide can be higher by carbon@CdS.

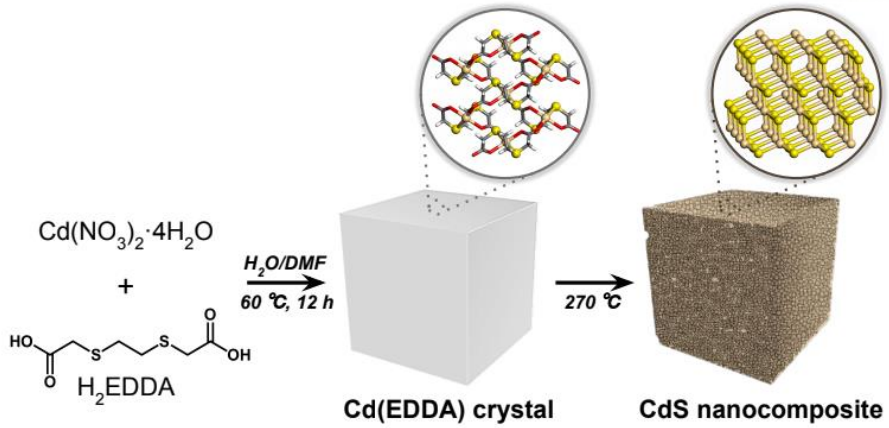

Figure 3.2. Synthetic scheme of MOF and transformation to CdS.

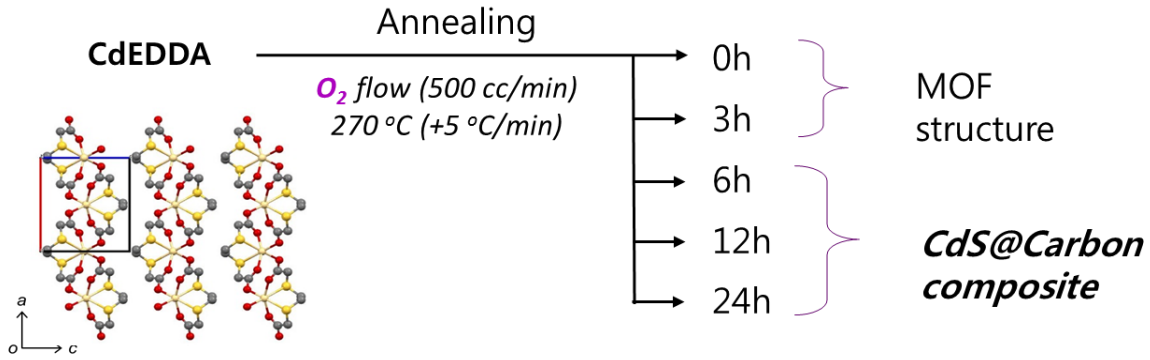

Figure 3.3. Synthetic scheme of MOF-derived carbon@CdS composite

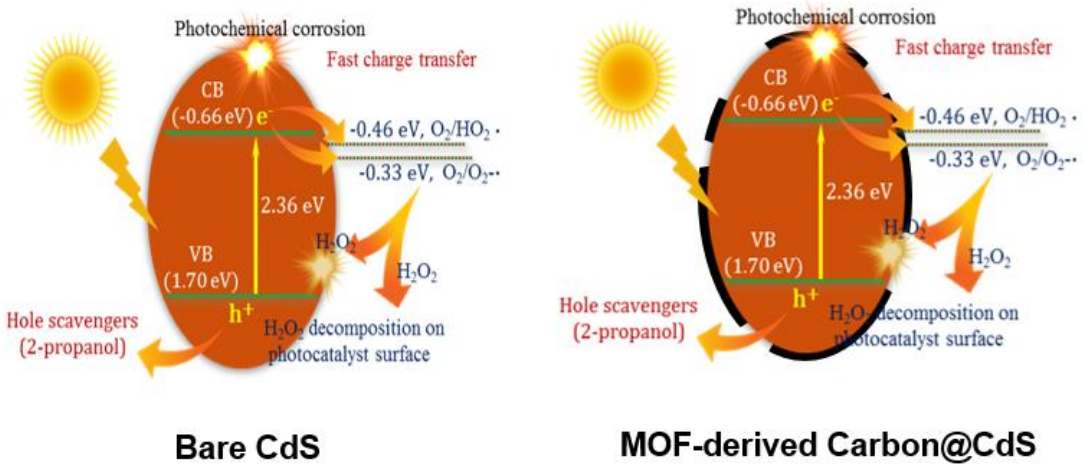

Figure 3.4. Schematic illustration of photocatalytic H_2O_2 generation on carbon encapsulated CdS surfaces.

3.3.2. Characterization of partially carbon encapsulated CdS

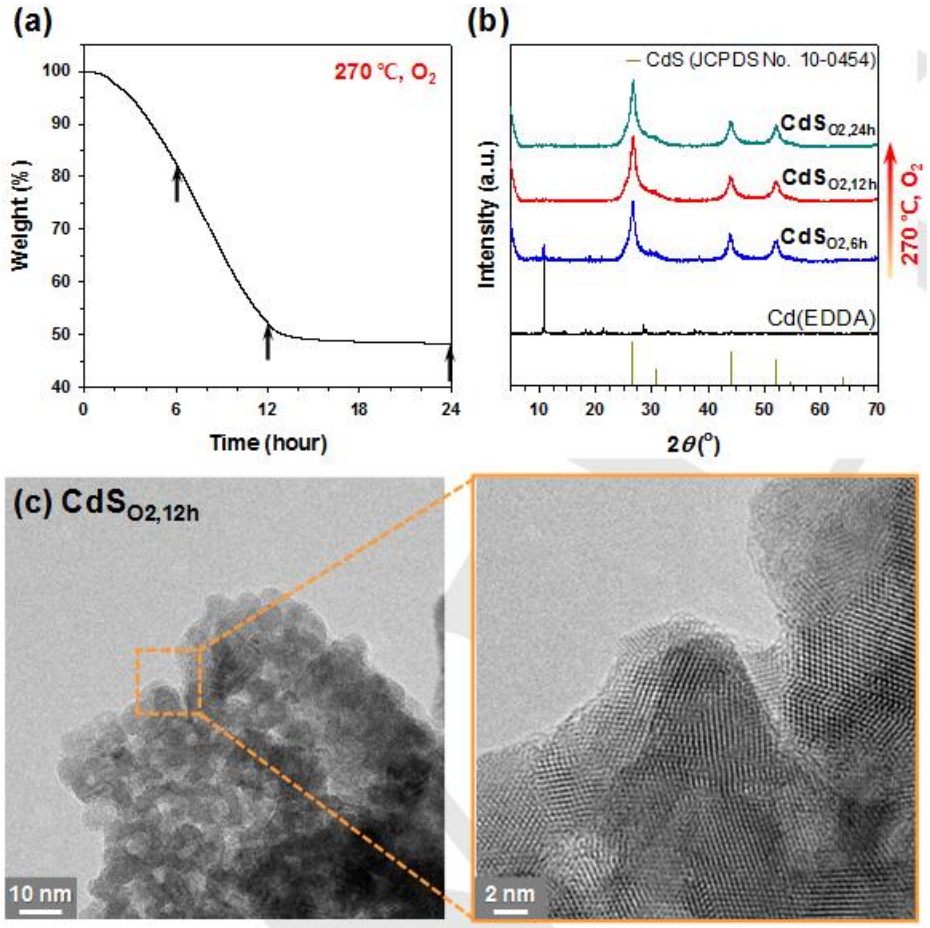

Figure 3.5. a) TGA of Cd(EDDA) at 270^{O}C under O_2 atmosphere. b) XRD pattern of MOF-derived CdS that were annealed for 24h, 12h, and 6h at oxygen atmosphere. C) TEM images MOF-derived CdS that were annealed for 12h at oxygen atmosphere with different magnification.

TGA in **Figure 3.5a** shows transformation of Cd(EDDA) to crystalline CdS at 270^{O}C in O_2 flow. It can be predicted that Cd(EDDA) annealed for 6 hours still has MOF structure because weight loss of it didn't severe. However, from the 12 hours of annealing, half of the weight of Cd(EDDA) was loss and there was not much difference of weight between 12h and 24h. It indicates that the states after transformation of two samples are similar. XRD patterns of MOF-derived samples were recorded in **Figure 3.5b**. The dark yellow peaks indicate CdS. In case of the Cd(EDDA), the MOF structure, CdS peaks cannot be found. As the time for annealing increased, the MOF structures disappeared. Transformation by 6h annealing makes the sample show single phase CdS structure but MOF structure still remains. However, after 12 hours of annealing, the MOF structure totally disappeared

and only CdS phase remains.

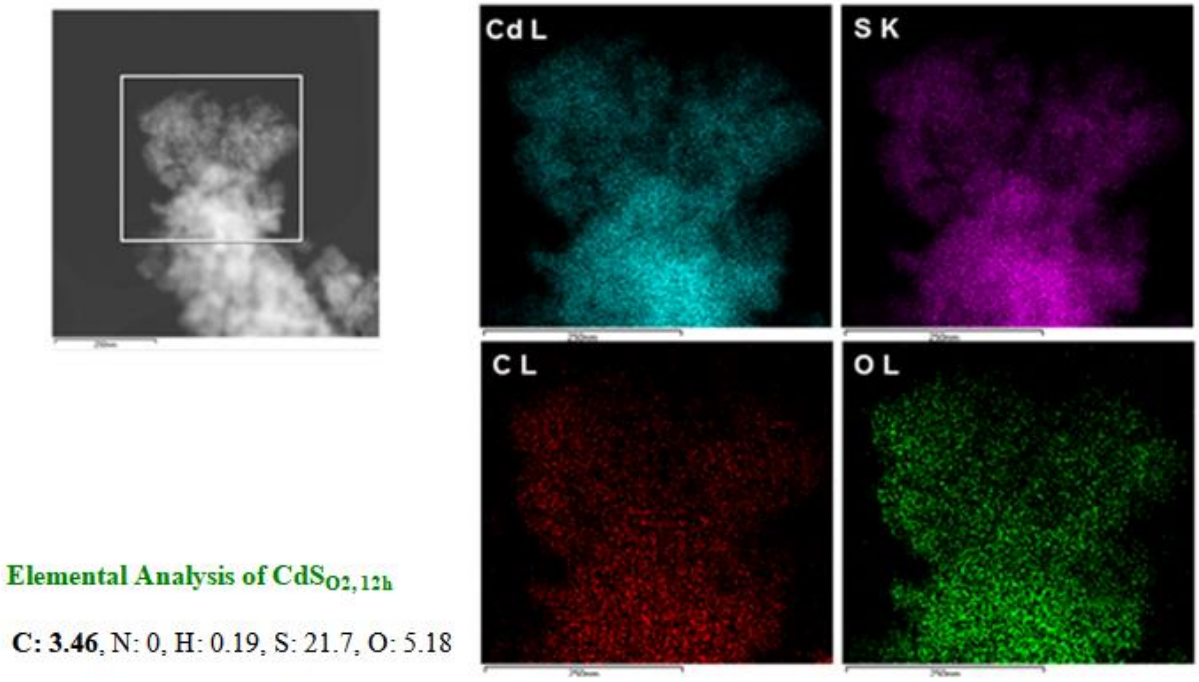

Figure 3.6. Elementary analysis of $CdS_{O2, 12h}$ and EDS mapping of MOF-derived CdS that were annealed for 12h at oxygen atmosphere. Cadmium (blue), sulfur (violet), carbon (red), and oxygen (green) are analyzed.

TEM images synthesized CdS is shown in **Figure 3.5c.** The lattice of $CdS_{O2, 12h}$ obviously appears and it means that the transformation from the MOF structure to CdS by longtime annealing without serious aggregation. On the other hand, carbon formed by carbonization of the organic ligand of MOF during annealing is hard to detect using TEM due to its low quantity. However, elementary analysis of $CdS_{O2, 12h}$ in **Figure 3.6** proved the existence of carbon. 3.46 wt% of carbon is found on the $CdS_{O2, 12h}$. In addition, EDS mapping in **Figure 3.6** also supports the existence of the carbon on the surface of the CdS generated by transformation of MOF structure by a long time of heat treatment. Cd and S components are detected by EDS mapping and well-dispersed carbon species and oxygen species can be observed. The oxygen species come from oxygen flow during annealing or the oxygen atoms from the carboxylates of the ligand of MOF structure before annealing and to identify their states, XPS spectra of $CdS_{O2, 12h}$ was recorded in **Figure 3.7.**

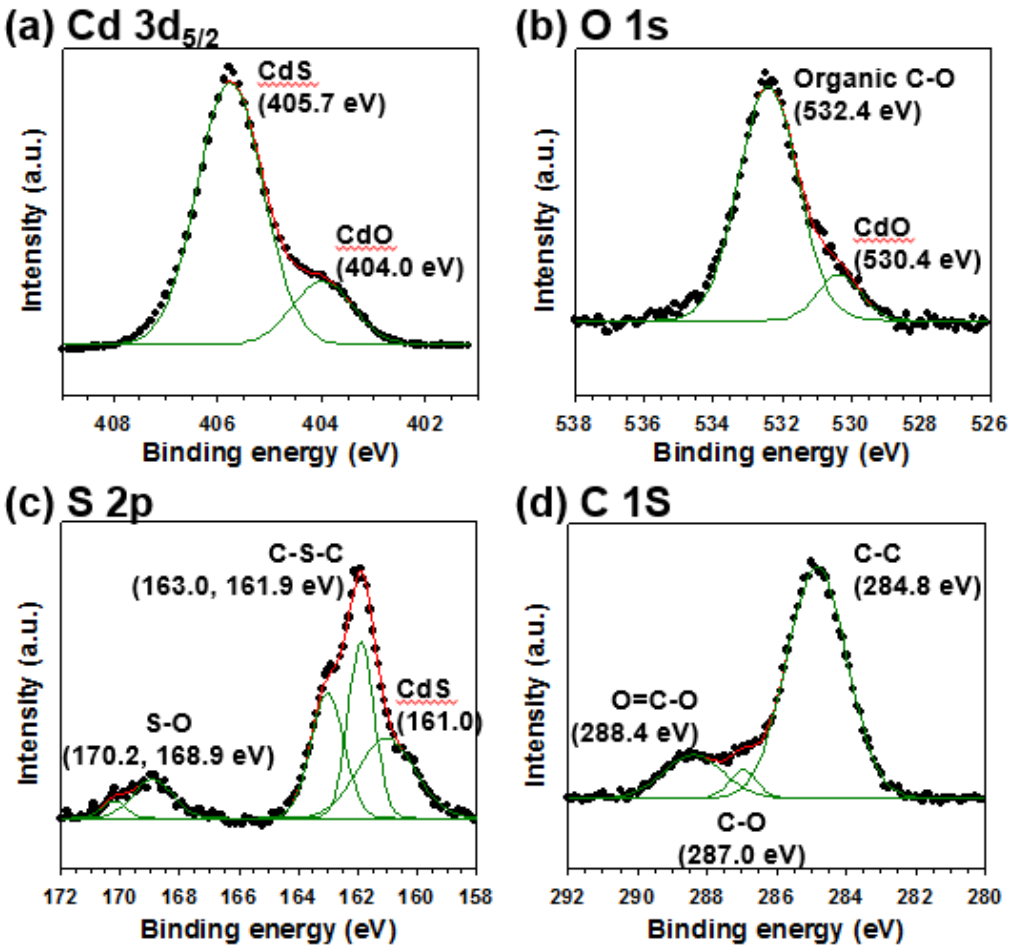

Figure 3.7. XPS spectra of a) Cd $3d_{5/2}$, b) S 2p, c) O 1s, and d) C 1s spectra of $CdS_{O2,\ 12h}$

The Cd $3d_{5/2}$, S 2p, O 1s, and C 1s spectra of $CdS_{O2,\ 12h}$ were measured by XPS. Both cadmium sulfide at 405.7 eV and cadmium oxide at 404.0 eV were detected in spectra of the Cd $3d_{5/2}$ and it is corresponding with the results of the detection of oxygen species in the EDS mapping. In addition, cadmium oxide also detected in spectra of the O 1S. Organic sulfur (C-S-C) at 163.0 and 161.9 eV and sulfate species (S-O) at 170.2 and 168.9 eV are observed in spectra of the S 2P as well as CdS peak. These spectra of the $CdS_{O2,\ 12h}$ indicate that CdS transformed from the MOF structure under oxygen atmosphere possess sulfur-doped polymeric carbon on the surface of the CdS.

3.3.3. Photocatalytic activity of MOF derived carbon@CdS for H_2O_2 production

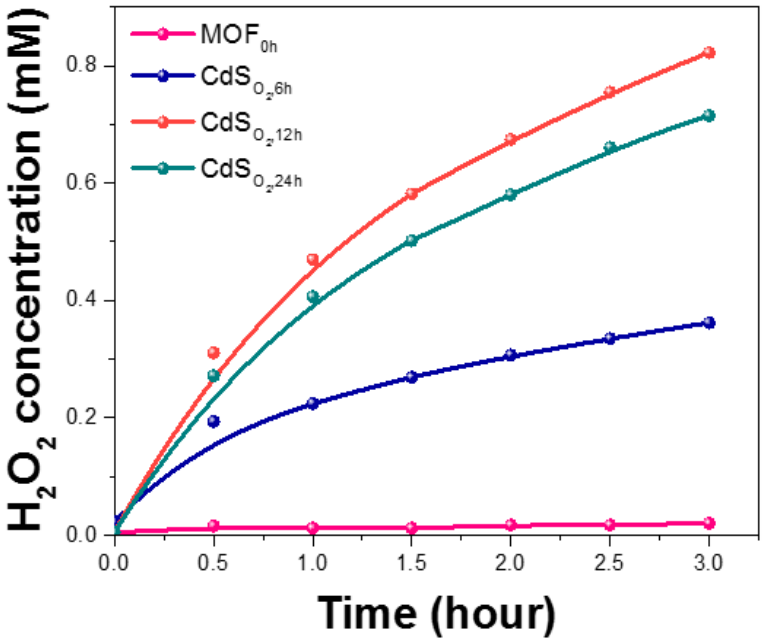

Figure 3.8. Photocatalytic hydrogen peroxide production of MOF-derived CdS annealed under oxygen atmosphere for 6h, 12h and 24h under visible light spectrum (λ > 420nm) in DI water without hole scavenger.

As-synthesized MOF-derived CdS with carbon matrix treated at 270 °C under oxygen atmosphere for a different time have been tested its ability to generate H_2O_2 photocatalytically at room temperature and pressure. The time-dependent photocatalytic H_2O_2 generations in deionized water have been summarized in **Figure 3.8.** MOF_{0h} sample which is a bare CdEDDA sample without any annealing process affirms the photo inactivity in the visible spectrum of light. The concentration of hydrogen peroxide generated by 0 hour annealed MOF is 0.02mM so, it is almost zero. On the other hand, a dramatic increase in photocatalytic H_2O_2 production was observed for CdS_{6h}, CdS_{12h}, and CdS_{24h} samples compared to MOF. These samples were obtained after 6, 12 and 24h annealing of the pure MOF sample in an oxygen atmosphere, respectively. These exceptional increases in H_2O_2 production attributed to the transformation of the organic ligand of MOF structure to carbon matrix on the surface of the CdS photocatalyst. The amount of produced H_2O_2 by all the CdS samples decreases as the time increases although the curve didn't reach to saturation point within 3 hours. After 3 hours from the test, the highest concentration of H_2O_2 was recorded as approximately 0.82mM at 3 hours by

the CdS_{12h}. The second record was 0.71mM of H_2O_2 at 3 hours generated by the CdS_{24h} and third one was 0.36mM by the CdS_{6h}. Thus, we concluded that the optimum annealing time under oxygen atmosphere is 12 hours for CdEDDA.

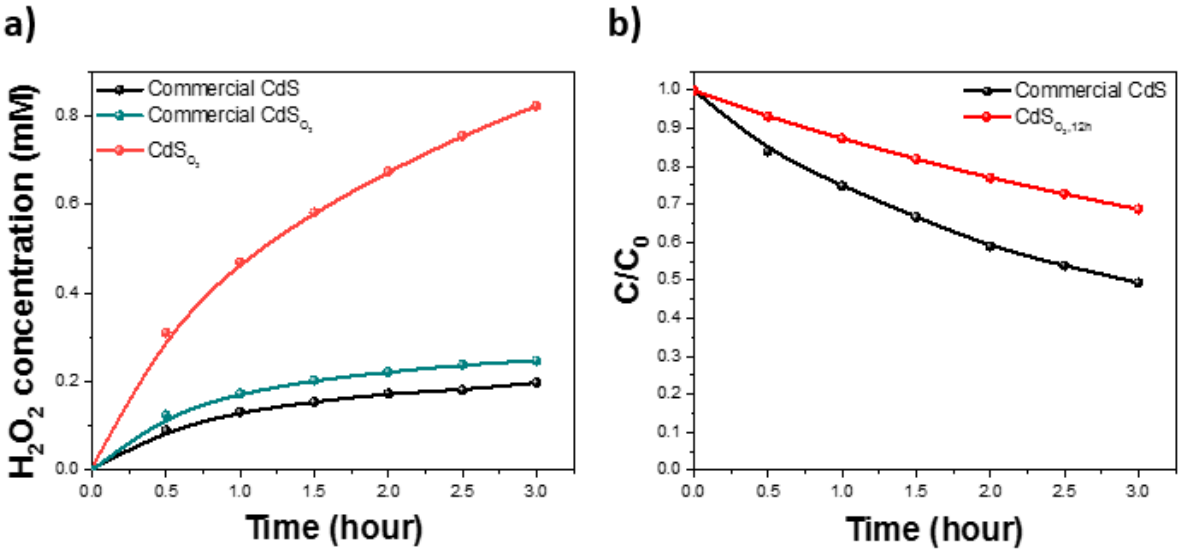

Figure 3.9. a) Photocatalytic hydrogen peroxide production of commercial CdS, commercial CdS annealed under O_2 atmosphere, MOF-derived CdS annealed under O_2 atmosphere for 12h under visible light spectrum (λ > 420nm) DI water without hole scavenger. b) Photocatalytic hydrogen peroxide decomposition by commercial CdS and, MOF-derived CdS annealed under O_2 atmosphere for 12h. The test was conducted in 1mM H_2O_2 solution under visible light spectrum (λ > 420nm).

To make comparative studies, three samples were tested their performance for forming hydrogen peroxide under visible light spectrum in the absence of electron donor in **Figure 3.9a**. The first commercialized CdS was used without any pretreatment while the second commercialized CdS was treated under oxygen atmosphere like MOF-derived CdS to clarify the role of the carbon matrix. The last samples were the optimized sample that was thermally treated at 270 °C for 12hours under oxygen atmosphere. The $CdS_{O2,\ 12h}$ was the best photoactive catalyst for producing H_2O_2 among three samples. The commercially available CdS shows the lowest activity. Its final concentration of hydrogen peroxide after 3 hours was 0.20mM. The final concentration of the $CdS_{O2,\ 12h}$ is 4.1 times higher than that of the commercial CdS. The concentration by thermally treated commercial CdS under oxygen was slightly increased compared to untreated CdS but still much lower than the $CdS_{O2,}$

$_{12h}$. These results well explain the role of the carbon matrix on the surface of the MOF-derived CdS. Oxygen treatment at high temperature itself didn't much effect to the photoactivity of the CdS photocatalyst. Only the sample that has carbon on the surface shows outstanding performance for the formation of H_2O_2. Thus, we expected that the carbon matrix is the key factor of fast H_2O_2 generation and slow H_2O_2 decomposition. So, decomposition rates of hydrogen peroxide of commercial CdS and $CdS_{O2,\ 12h}$ under visible light range were also compared in **Figure 3.9b**. Half of the pre-existed hydrogen peroxide was degraded from 1mM by commercial CdS under visible light irradiation at 3 hours of the test. On the other hand, $CdS_{O2,\ 12h}$ shows much lower activity to decompose the hydrogen peroxide. Around 70 % of H_2O_2 remains by the $CdS_{O2,\ 12h}$ during the test. The degradation rate of hydrogen peroxide for $CdS_{O2,\ 12h}$ is clear evidence that carbon matrix on the surface of MOF-derived CdS can protect hydrogen peroxide from degradation.

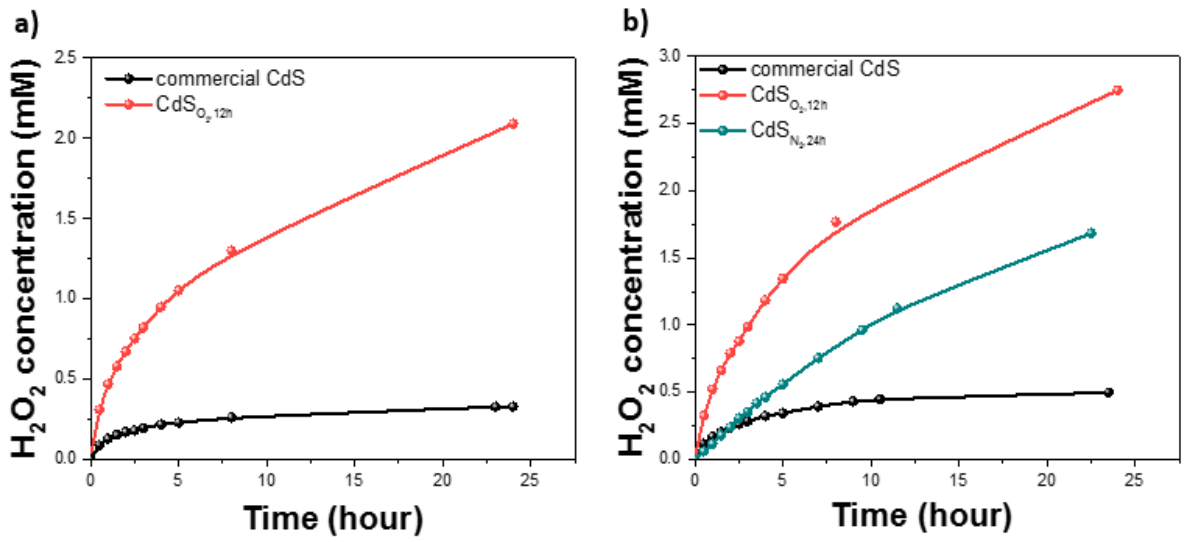

Figure 3.10. a) Photocatalytic hydrogen peroxide production of commercial CdS and, MOF-derived CdS annealed for 12h under O_2 atmosphere under visible light spectrum (λ > 420nm) in DI water without hole scavenger, b) Photocatalytic hydrogen peroxide production of commercial CdS and, MOF-derived CdS annealed under O_2 atmosphere for 12h under visible light spectrum (λ > 420nm) in 10% 2-propanol solution.

The ability to generate hydrogen peroxide of $CdS_{O2,\ 12h}$ is tested for 24hours in **Figure 3.10** with (**Figure 3.10a**) and without (**Figure 3.10b**) presence of the sacrificial agent, 2-propanol, and under visible light, because the concentration of H_2O_2 during the 3 hours of the reaction didn't

draw saturation curve yet. In **Figure 3.10a**, the H_2O_2 concentration of the $CdS_{O2,\ 12h}$ sample reach to 2.09mM at 24 hours of reaction. It is 6.33 times higher value than that of commercial CdS. Even the $CdS_{O2,\ 12h}$ sample didn't fully-saturated until 24 hours after it started to produce hydrogen peroxide while commercialized CdS was almost saturated after 8 hours. Both samples in **Figure 3.10b** generate a higher amount of H_2O_2 than they produced in the absence of the sacrificial agent. 2.75mM of H_2O_2 was produced by CdS_{12h} and around 0.5mM of H_2O_2 was produced by the commercial CdS respectively when 2-propanol exists in the solution. MOF-derived carbon@CdS also still generate H_2O_2 without saturation at 24 hours. The concentration difference between the samples dispersed in different solution provides evidence that H_2O_2 formation reaction is not originated from water oxidation reaction but the oxygen reduction reaction because 2-propanol is a hole scavenger and it reacts with the photogenerated holes. If hydrogen peroxide is synthesized from the water oxidation, it is hard to be generated in the presence of hole scavenger for the reason that the holes have to be reacted with water to produce H_2O_2 instead of 2-propanol. A CdS_{N2} sample was tested to check the effects of a quantity of the carbon matrix on the photocatalyst. If the MOF is annealed under N_2 condition, a larger quantity of the carbon matrix is formed on the photocatalyst than O_2 condition. So, MOF-derived CdS was synthesized under nitrogen atmosphere for 6, 12, 24 and 48 hours and found the best sample for producing hydrogen peroxide. As a result, the MOF-derived CdS annealed for 24 hours was the best sample. Elemental analysis proved that the CdS treated under a nitrogen atmosphere for 24 hours contains 9.11 percent of the carbon while the CdS treated under an oxygen atmosphere for 12 hours contains 3.46 percent of the carbon. The $CdS_{N2,\ 24h}$ also tested its H_2O_2 production ability under visible light in 10% 2-propanol solution. The final concentration by CdS_{N2} was much lower than that of CdS_{O2} but the concentration curve drew a much more linear line than the concentration curve by CdS_{O2}. From this result, we concluded that thick carbon matrix helps to the steady generation of H_2O_2 with the same amount but it also blocks the active site of the CdS and hinders the absorbance of the light. The main role of the carbon matrix is obviously preventing the degradation of hydrogen peroxide but activity can be changed by its quantity.

Figure 3.11 shows the photoactivity of commercial CdS and $CdS_{O2,\ 12h}$ for 1 hour of the experiment (a) and for 3 hours of experiment (b). In both case, the ability to generate H_2O_2 is decreasing as time goes by. Although all samples show better activity when the electron donor is added in the solution, the results that are conducted without an electron donor are comparable. Activity differences aren't much reduced by the presence of 2-propanol and it indicates that the surface properties of both commercialized CdS and $CdS_{O2,\ 12h}$ are good for the O_2 reduction reaction. **Table 3.1** summarizes the

results for photocatalytic H_2O_2 production by various metal-based photocatalysts under visible light irradiation from various literature. The activity of our sample shows quite higher value among the metal-based photocatalyst for H_2O_2 production. 523 μmol of H_2O_2 is produced by 1 g of $CdS_{O2,\ 12h}$ for 1 hour and it is comparable value with the highest one (547 μmol g_{cat}^{-1} h^{-1} by $Cd_3(C_3N_3S_3)_2$).

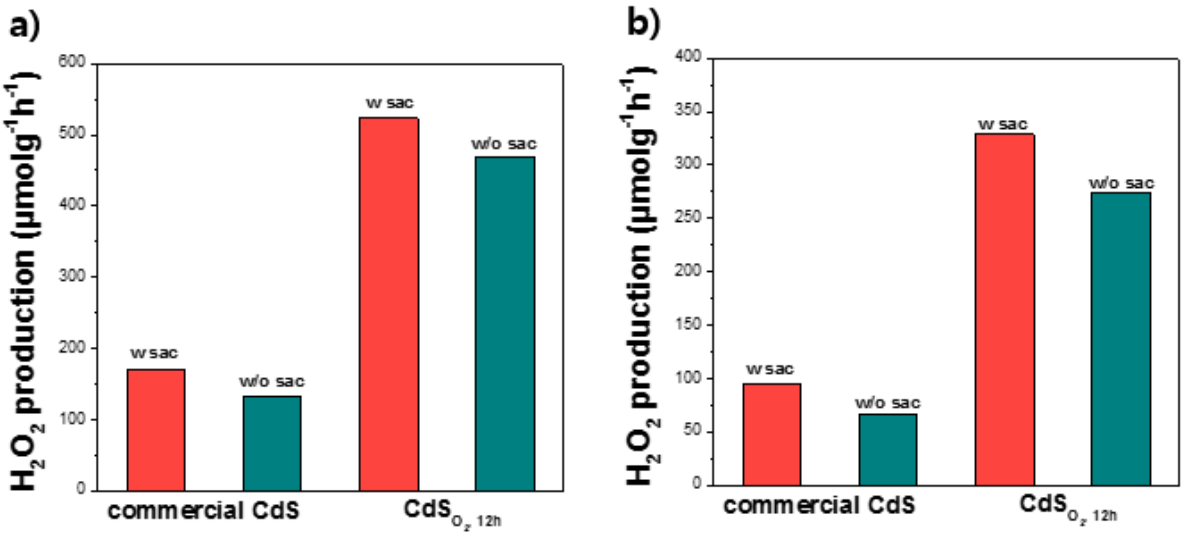

Figure 3.11. a) Hydrogen peroxide production rate for 1 hour of photoreaction by commercial CdS and $CdS_{O2,\ 12h}$ with and without a sacrificial agent (2-propanol). b) Hydrogen peroxide production rate for 3 hours of photoreaction by commercial CdS and $CdS_{O2,\ 12h}$ with and without a sacrificial agent (2-propanol).

Table 3.1. Comparison of selected photocatalysts for visible-light-driven H_2O_2 production from H_2O and O_2.

Catalysts	Activity [μmol g_{cat}^{-1} h^{-1}] [a]	Reaction time [h][b]	Ref.
Commercial CdS	171	8	This work
$CdS_{O2,12h}$	523	> 24	This work
$Au/BiVO_4$	2.4	10	[16]
Au Ag/TiO_2	283	12	[17]
$Cd_3(C_3N_3S_3)_2$	547	4	[18]
CdS-graphene	10.7	12	[19]
BM/Au-TiO_2	320±30	1	[20]
SN-GQD/TiO_2	110	1.5	[21]

For an accurate comparison, gravimetric activity was acquired from the published data by using the mass of the entire photocatalyst and the amount of produced H_2O_2 until saturation. Saturation time was estimated from the published data of photocatalytic H_2O_2 formation unless directly mentioned in the literature.

3.4. Conclusion

In summary, we synthesized carbon@CdS photocatalyst from the MOF structure. The MOF was used as a template as well as the precursor of the photocatalyst. The cadmium-based MOF contains S in the organic ligand of MOF structure and after annealing, it is destructed and transformed to single-phase CdS photocatalyst that has carbon matrix formed by carbonization of the organic ligand of MOF on the surface of the CdS. The carbon matrix of the photocatalysts partially-encapsulates the surface and prevents the H_2O_2 to be decomposed by inhibiting the adsorption on the surface of the photocatalyst and oxidation reaction with photo-generated holes. Besides, carbon encapsulation helps to reduce electron-hole recombination [22, 23]. Thus, its photoactivity is enhanced compared to bare CdS photocatalyst. The MOF-derived carbon@CdS produced 6 times higher hydrogen peroxide than commercial CdS for 24 hours of the photo-reaction. The carbon@CdS also restrict fast saturation of generated H_2O_2. For commercial CdS, the concentration of H_2O_2 is almost saturated from 8 hours of the photoreaction but for MOF-derived carbon@CdS, H_2O_2 didn't saturate during the 24 hours of the photoreaction.

3.5. References

[1] Yong-Jun Yuan, Daqin Chen, Zhen-Tao Yu and Zhi-Gang Zou. J. *Mater. Chem. A*, **2018**, 6, 11606

[2] J. R. Darwent and G. Porter, J. Chem. Soc., *Chem. Commun*.,**1981**, 145–146.

[3] Lei Cheng, Quanjun Xiang, Yulong Liao and Huaiwu Zhang. Energy Environ. Sci., **2018**, 11, 1362

[4] D. Meissner, R. Memming, and B. Kastening, *Journal of Physical Chemistry*, **1988,** 92, 12, pp. 3476–3483.

[5] Wenlong Zhen, Xiaofeng Ning, Baojun Yang, Yuqi Wu, Zhen Li, Gongxuan Lu. *Applied Catalysis B: Environmental*, **2018**, 221, 243–257

[6] D. Wang et al. *Journal of Environmental Chemical Engineering*, **2015**, 3, 1578–1585

[7] Mengye Wang, Lejuan Cai, Yi Wang, Feichi Zhou, Kang Xu, Xiaoming Tao, and Yang Chai., *J. Am. Chem. Soc*. **2017**, 139, 4144−4151

[8] D. Zhang et *al*. *Applied Surface Science*. **2017**, 420, 161–166

[9] D. Tian, Q. Chen, Y. Li, Y.-H. Zhang, Z. Chang and X.-H. Bu, *Angew. Chem., Int*. Ed., **2014**, 53, 837 -841

[10] Qi Yu, Hong Dong, Xin Zhang, Ya-Xin Zhu, Jian-Hui Wang, Feng-Ming Zhang and Xiao-Jun Sun. *CrystEngComm*, **2018**, 20, 3228

[11] Ying Li, Hua Xu, Shuxin Ouyangab and Jinhua Ye. *Phys. Chem. Chem. Phys*., **2016**, 18, 7563-7572

[12] Caihong Zhang, Lunhong Ai and Jing Jiang. *J. Mater. Chem. A*, **2015**, 3, 3074-3081

[13] Jasmina Hafizovic Cavka, Søren Jakobsen, Unni Olsbye, Nathalie Guillou, Carlo Lamberti, Silvia Bordiga and Karl Petter Lillerud. *J. Am. Chem. Soc*. **2008**, 130, 42, 13850-13851

[14] Yanghe Fu, Dengrong Sun, Yongjuan Chen, Renkun Huang, Zhengxin Ding, Xianzhi Fu, Zhaohui Li. *Angew. Chem. Int*. Ed.**2012**, 51, 3364 –3367

[15] Amarajothi Dhakshinamoorthy, Zhaohui Li and Hermenegildo Garcia. *Chem. Soc. Rev*., **2018**, 47, 8134-8172

[16] Hiroaki Hirakawa, Shingo Shiota, Yasuhiro Shiraishi, Hirokatsu Sakamoto, Satoshi, Ichikawa,

and Takayuki Hirai. *ACS Catal.* **2016**, 6, 8, 4976-4982

[17] Daijiro Tsukamoto, Akimitsu Shiro, Yasuhiro Shiraishi, Yoshitsune Sugano, Satoshi Ichikawa, Shunsuke Tanaka, and Takayuki Hirai. *ACS Catal.* **2012**, 2, 4, 599-603

[18] Huaqiang Zhuang, LifangYang, Jie Xu, Fuying Li, Zizhong Zhang, Huaxiang Lin, Jinlin Long, and Xuxu Wang. *Scientific Reports* | 5:16947 | DOI: 10.1038/srep16947

[19] Suman Thakur, Tolendra Kshetri, Nam Hoon Kim, Joong Hee Lee. *Journal of Catalysis.* **2017**, 345**,** 78–86

[20] Miwako Teranishi, Riyoko Hoshino, Shin-ichi Naya, Hiroaki Tada. *Angew. Chem. Int. Ed*. **2016**, 55, 12773–12777

[21] Longhui Zheng, Hanrui Su, Jingzhen Zhang, Laxman S.Walekar, Hamed Vafaei Molamahmood, Baoxue Zhou, Mingce Long, Yun Hang Hu. *Applied Catalysis B: Environmental*. **2018**, 239, 475-484

[22] C. H. Choi, M. Kim, H. C. Kwon, S. J. Cho, S. Yun, H.-T. Kim, K. J.J. Mayrhofer, H. Kim, M. Choi, *Nat. Commun*. **2016**, 7, 10922

[23] C. H. Choi, H. C. Kwon, S. Yook, H. Shin, H. Kim, M. Choi, *J. Phys. Chem. C*, **2014**, 118, 30063-30070.

4. Solar Light Assisted Reductive Hydrogen Peroxide Production by Graphitic Carbon Nitride Photocatalyst from Dioxygen and Water

4.1. Introduction

4.1.1. Graphitic Carbon nitride (g-C_3N_4)

Graphitic Carbon nitride (g-C_3N_4) is a promising two-dimensional triazine- or heptazine-based conjugated polymer. It is considered as a good alternative for toxic metal-containing photocatalysis due to its metal-free characteristics and other suitable properties such as low-cost, robust, and visible-light-activity since photocatalytic hydrogen production of g-C_3N_4 under visible light was reported by Wang et *al* in 2009 [1, 2]. Its high stability (chemically in acid, base and organic solvents and thermally up to 600 °C in air), tunable electronic structure, abundance, and proper band gap position (overall: 2.7 eV, CB: -1.12 eV vs. SHE and VB: +1.6 eV vs. SHE) also main advantages for photocatalyst [2, 3]. The electrons and holes generated separately as well as, oxidation and reduction reaction can occur on nitrogen and carbon atoms respectively in g-C_3N_4 because VB of g-C_3N_4 is mainly composed of nitrogen P_Z orbitals and CB of g-C_3N_4 are mainly composed of carbon P_Z orbitals [4]. Although g-C_3N_4 has promising potential as a photocatalysis, the photocatalytic activity of pristine g-C_3N_4 is still low. Quantum efficiency of g-C_3N_4 is around 0.1% at 420 – 460 nm range. This reason is originated from the small specific surface area, marginal optical absorption in the visible region, fast rate of charge recombination, and low electric conductivity of g-C_3N_4 [5]. To increase its performance, many strategies such as doping [6, 7], making a heterojunction [8, 9], and defects engineering [10] have been studied.

Additionally, the g-C_3N_4 is suitable photocatalyst to produce hydrogen peroxide so, many efforts have been done by researchers. For example, Yasuhiro Shiraishi et *al* prepared g-C_3N_4 that has high surface area through polymerization of urea or silica-templated polymerization of cyanamide and found that g-C_3N_4 selectively produces hydrogen peroxide promoting the selective two-electron reduction of O_2 in presence of the alcohol and oxygen due to the efficient formation of 1,4-endoperoxide species on its surface [11]. Shuna Li et al prepared g-C_3N_4 that has carbon vacancies on the surface of it by calcination with Ar gas. This g-C_3N_4 efficiently reduced oxygen gas to hydrogen peroxide under visible irradiation without using any precious metal co-catalysts or organic scavengers [12].

4.1.2. Ionothermal synthesis of carbon nitride (salt-melts method)

The problem of the imide-bridged heptazine units based melon-type g-C_3N_4 synthesized by usual thermal condensation method is its low crystallinity. Bulk synthesis process produces less condensed and less crystalline g-C_3N_4 due to incomplete condensation or polymerization in the bulk and it results in the kinetic problem [13]. Besides, g-C_3N_4 bear sluggish exciton dissociation like other conjugated polymers because of the intrinsic strong Coulomb interactions of Frenkel excitons resulting in high exciton binding energy [14]. Thus, bulk g-C_3N_4 usually shows moderate photocatalytic performance and low crystalline g-C_3N_4 contains many defects that act as a recombination center and a terminal unreacted amino group.

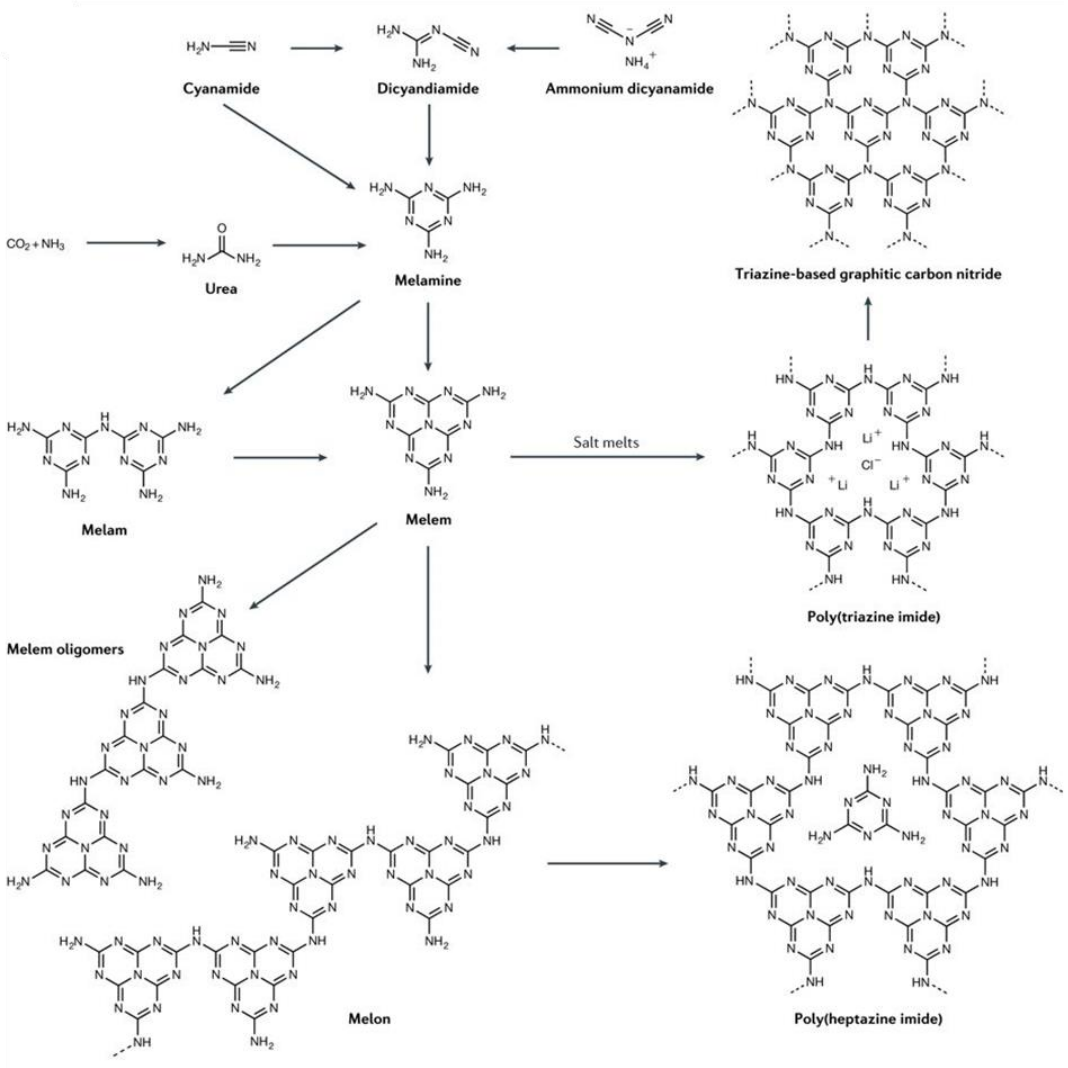

Figure 4.1 Structures of the precursors and g-C_3N_4 *via* various synthesis method [20].

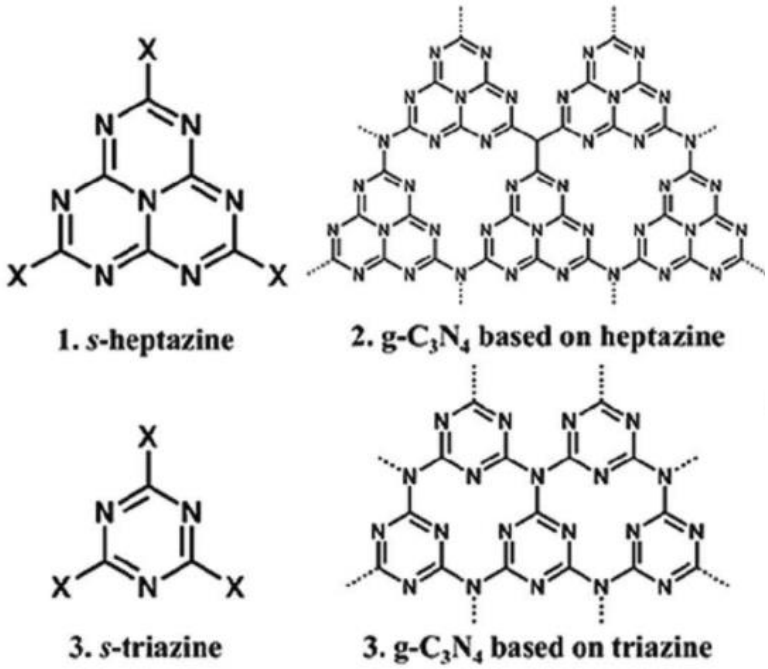

Figure 4.2. The structures of s-heptazine, s-triazine, heptazine-based g-C_3N_4 and triazine-based g-C_3N_4 [1].

To form highly crystalline and condensed 2D g-C_3N_4, ionothermal synthesis method with salt melt like LiCl and KCl are conducted. The LiCl - KCl salt mixture is usually used chemicals in this process because these are stable at high temperature, non-corrosive and lower melting point (352^{o}C) than the polycondensation point of s-heptazine (400^{o}C and above) [15]. These molten salts form solvent and accelerate the polymerization of g-C_3N_4, tailor the properties and structure of the polymer and even change the polymerization route [16, 17]. Consequently, this method synthesizes the g-C_3N_4 that has improved the degree of condensation, high crystallinity, and fewer defects [14] and it prefers to make triazine-based structure in the presence of lithium [17]. However, heptazine-based g-C_3N_4 has larger π-conjugated system compared with triazine-based g-C_3N_4 and it indicates that for light-harvesting and enhanced carrier mobility, heptazine-based g-C_3N_4 is better than triazine-based g-C_3N_4 [18] . Therefore, the synthesis method for heptazine-based g-C_3N_4 is developing [19].

In this study, graphitic carbon nitride was synthesized *via* ionothermal synthesis of urea precursor with KCl/LiCl eutectic mixture. Hydrogen peroxide is generated by this g-C_3N_4 under visible light irradiation with 2-propanol as a sacrificial agent.

4.2. Experimental

4.2.1. g-C_3N_4 synthesis

Preparation of g-C_3N_4 *via* ionothermal synthesis.

Typically, urea (min. 99.0% m/m, Junsei) was chosen as a precursor of g-C_3N_4. 10g of urea was mixed with 2.7g of LiCl (anhydrous, 99%, Sigma-Aldrich) and 3.3g of KCl (anhydrous, ≥ 99%, Sigma-Aldrich). Then, the mixture was fully-grinded by mortar. After grinding, the solid powder was transferred to combustion boat and the boat was covered with aluminum foils. Then, it was heated in box furnace at 823K with a heating rate of 5 K / min for two hours. The g-C_3N_4 powder was collected after the temperature of the furnace cooled down to room temperature. Then to remove the metal residues in g-C_3N_4 from the salts, collected g-C_3N_4 powder was washed and filtrated with 6 L of preheated warm deionized water. After filtration, the solids were dried inside an oven for overnight and ground again by the mortar before performance test.

Preparation of g-C_3N_4 *via* thermal condensation.

For comparison, g-C_3N_4 through thermal condensation was synthesized. The urea was also selected as a precursor. 10 g of urea is fully-grinded by mortar and then ground solids moved to the container and heated in the box furnace at 823K with a heating rate of 5 K / min for two hours. The g-C_3N_4 powder was collected after the temperature of the furnace cooled down to room temperature and ground again by the mortar before performance test.

4.2.2 Photocatalytic performance of g-C_3N_4

Photocatalytic production of H_2O_2 by g-C_3N_4.

Photocatalytic activity of g-C_3N_4 synthesized by thermal condensation and ionothermal method samples to produce hydrogen peroxide were evaluated at room temperature and pressure. 0.025g of photocatalyst powder was dispersed in 25 ml of deionized water in the presence of sacrificial agent 2-propanol. The colloidal solution in the reactor was purged with oxygen gas for half hour to saturate the oxygen in the dark condition. The performance test of the H_2O_2 production was carried out with 300W Xenon lamp with continuous oxygen bubbling and to maintain dispersion, solution was stirred by magnetic stirrer before and during reaction. The photocatalyst samples were tested under visible light irradiation with 420nm cut-off filter. 0.6 mL of sample was collected at every sampling during the 24 hours reaction by a syringe and filtrated by 0.45 μM PTFE syringe filter (Millex).

Quantity optimization

To clarify the concentration difference by dispersed photocatalyst in the solution, 0.005 g, 0.01g, 0.025g, 0.04g, 0.0625g and 0.125g of photocatalyst powder was dispersed in 25 ml of deionized water in the presence of sacrificial agent 2-propanol. The colloidal solution in the reactor was purged with oxygen gas for half hour to saturate the oxygen in the dark condition. The performance test of the H_2O_2 production was carried out with 300W Xenon lamp with continuous oxygen bubbling and to maintain dispersion, solution was stirred by magnetic stirrer before and during reaction. The photocatalyst samples were tested under visible light irradiation with 420nm cut-off filter. 0.6 mL of sample was collected at every sampling during the 24 hours reaction by a syringe and filtrated by 0.45 μM PTFE syringe filter (Millex).

4.3. Results & discussions

4.3.1. Photochemical reductive H_2O_2 production on g-C_3N_4

The g-C_3N_4 can be synthesized from various precursors that are containing carbon and nitrogen atoms such as melamine ($C_3H_6N_6$), cyanamide (CH_2N_2), dicyandiamide ($C_2H_4N_4$), urea (CH_4N_2O) and thiourea (CH_4N_2S). Among the many precursors, widely used two precursors, melamine and urea, was selected to synthesize g-C_3N_4 through bulk thermal polymerization. Two precursors were treated under the same reaction condition. Two kinds of g-C_3N_4 from different precursors were tested its photoactivity to generate hydrogen peroxide under visible light irradiation with the same condition in **Figure 4.3**. The results revealed that g-C_3N_4 from urea produces a slightly higher amount of hydrogen peroxide. So from the next experiment, urea was used as a precursor for synthesizing g-C_3N_4. Then two types of g-C_3N_4 were synthesized *via* two different methods. To make more crystalline structured g-C_3N_4, ionothermal polymerization method with two salt-melts (LiCl and KCl) was used for urea precursor. Two g-C_3N_4 from different synthesizing method were tested its performance to produce hydrogen peroxide in **Figure 4.4a**. The concentration of generated H_2O_2 was extremely increased by molten salt synthesis. The g-C_3N_4 synthesized by molten-salt method generates 16.2 times higher concentration of hydrogen peroxide compared to g-C_3N_4 that synthesized by bulk condensation and it is not saturated until 24 hours of the experiment. Then, their decomposition rate of hydrogen peroxide was tested under 1 sun condition in **Figure 4.4b**. Only 1.12% of hydrogen peroxide was degraded if a photocatalytic reaction doesn't occur. Two g-C_3N_4 made by the different method has a similar ability to decompose hydrogen peroxide while g-C_3N_4 from ionothermal polymerization shows better photoactivity to generate it. In both cases, about 11% of the hydrogen peroxide was decomposed for 1 h of the reaction.

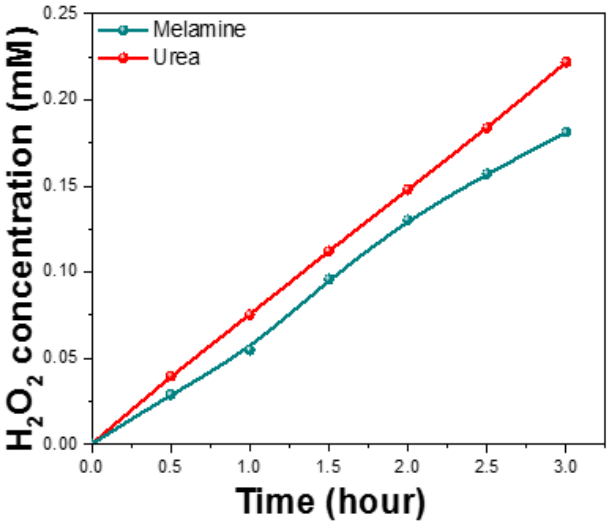

Figure 4.3. Photocatalytic hydrogen peroxide production by g-C_3N_4 synthesized from different precursors *via* thermal condensation under visible light spectrum (λ > 420nm) in 10% 2-propanol solution.

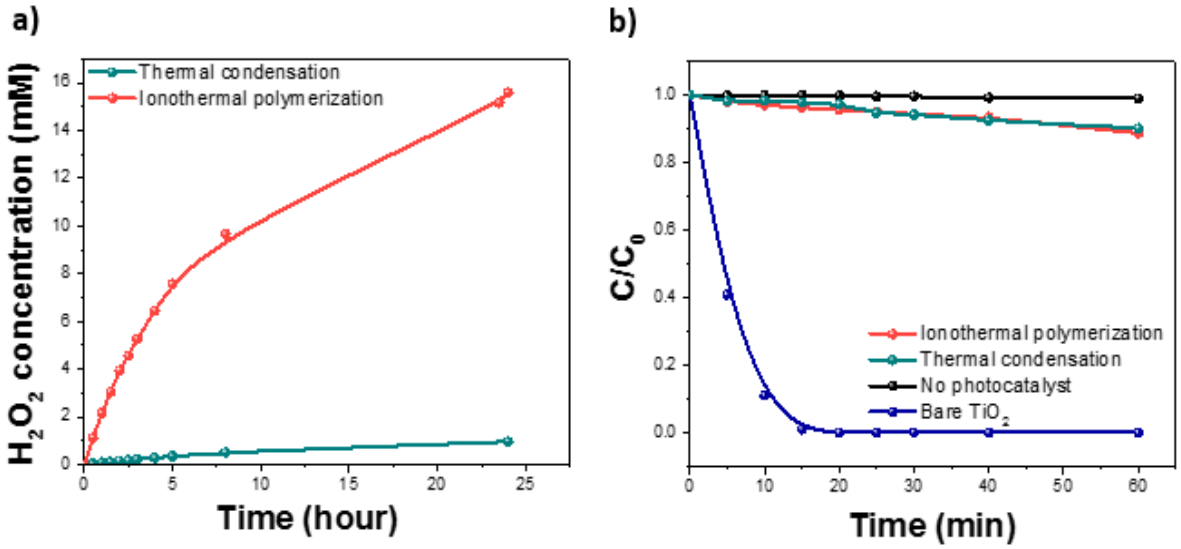

Figure 4.4. a) Photocatalytic hydrogen peroxide production by g-C_3N_4 *via* thermal polymerization and ionothermal polymerization under visible light spectrum (λ > 420nm) in 10% 2-propanol solution. b) Photocatalytic hydrogen peroxide decomposition by g-C_3N_4 *via* thermal polymerization and ionothermal polymerization under 1 sun spectrum (100mW/cm^2) with 1 sun cut-off filter in 10% 2-propanol solution.

The g-C_3N_4 synthesized by ionothermal condensation has good photoactivity under visible light and in presence of 2-propanol that acts as a hole scavenger. However, its performance is close to zero when there is no electron donors in the solution if **Figure 4.5**. These results indicates that the surface kinetics of g-C_3N_4 is very poor and surface recombination is severe problem of this photocatalyst. To overcome low surface kinetics of g-C_3N_4, co-catalyst loading may applied. Platinum is a common co-catalyst for photocatalyst and some literature [21, 22] mentioned that single-Pt loading on the surface of the photocatalyst improve the H_2O_2 generation ability. The g-C_3N_4

synthesized molten-salt method was tested with different quantities in **Figure 4.6**. As the concentration of catalyst increases from 0.2 g/L to 1.6 g/L, concentration of the hydrogen peroxide also increases in **Figure 4.6a**. However, higher concentration than 1.6 g/L of photocatalyst, 2.5 g/L of g-C_3N_4, doesn't produce larger amount of H_2O_2. Thus, optimum quantity of the photocatalyst is 1.6 g/L. On the other hand, H_2O_2 production rates per weight of the catalyst and hour show a tendency to decrease as the catalyst concentration increases in **Figure 4.6b**. Then, H_2O_2 production performance of the quantity-optimized g-C_3N_4 was tested under 1 sun irradiation and under visible light irradiation in **Figure 4.7a**. Concentration of produced H_2O_2 is around 1.6 times higher in 1 sun irradiation due to utilization of the UV region. Finally, remarkable amount of H_2O_2 that was about 20mM was produced after 24 hours of the reaction under 1sun irradiation while bulk g-C_3N_4 *via* thermal condensation generated only 1.12mM of it in **Figure 4.10b**.

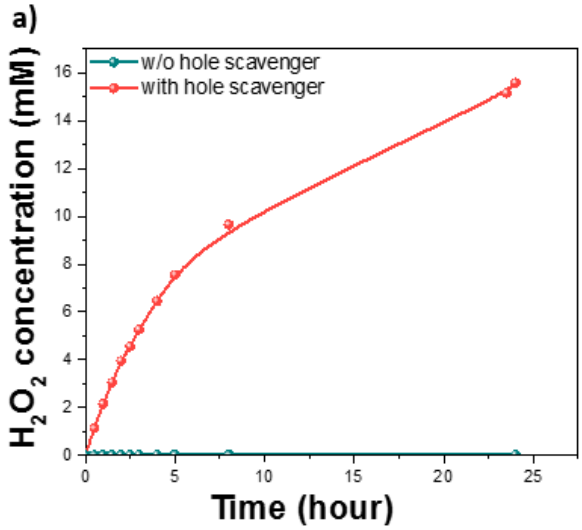

Figure 4.5. Photocatalytic hydrogen peroxide production by g-C_3N_4 *via* ionothermal polymerization under visible light spectrum (λ > 420nm) in 10% 2-propanol solution and in pure DI water respectively.

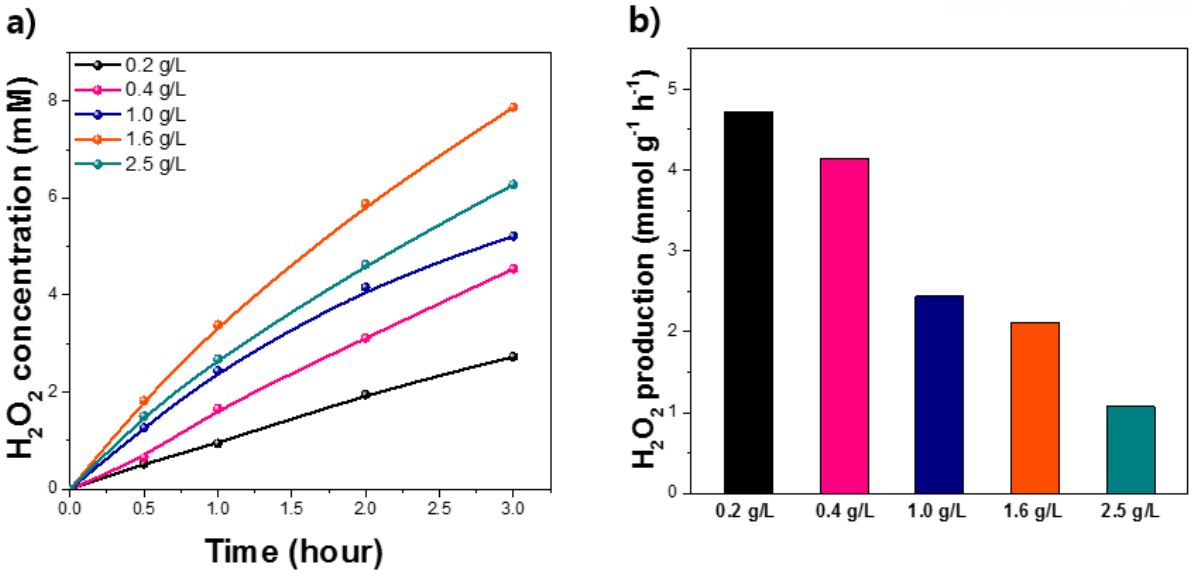

Figure 4.6. a) quantity optimization of g-C_3N_4 *via* ionothermal polymerization (0.2 g/L, 0.4 g/L, 1 g/L, 1.6 g/L and, 2.5 g/L) and b) normalization of g-C_3N_4 *via* ionothermal polymerization (0.2 g/L, 0.4 g/L, 1 g/L, 1.6 g/L and, 2.5 g/L) under visible light spectrum (λ > 420nm) in 10% 2-propanol solution.

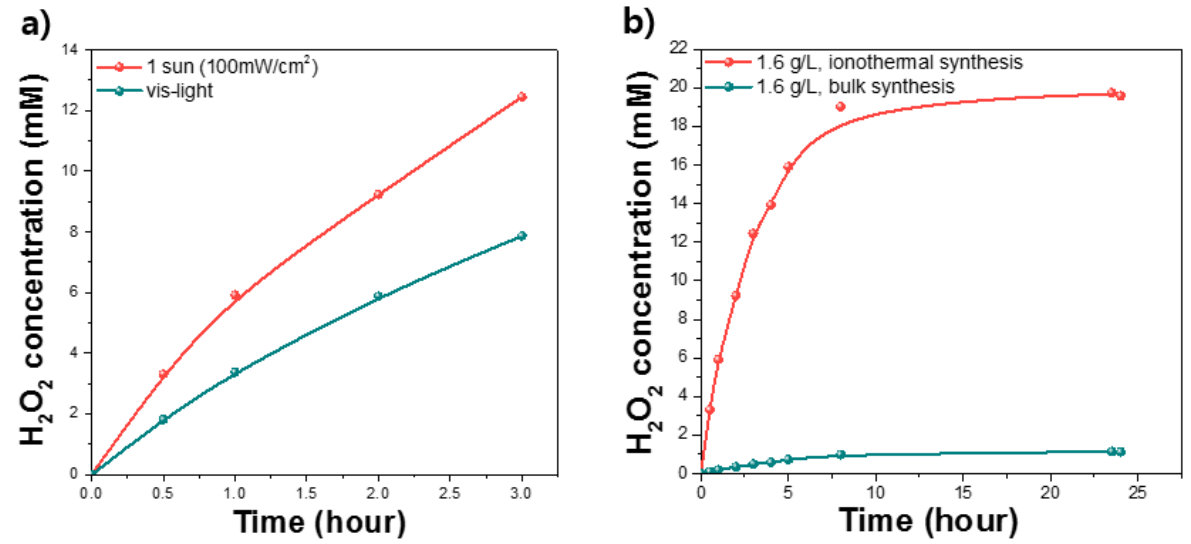

Figure 4.7. a) H_2O_2 concentration of the quantity-optimized g-C_3N_4 under 1 sun irradiation and under visible light in presence of 10% 2-propanol. b) Comparison of H_2O_2 concentration by g-C_3N_4 synthesized *via* molten-salt method and thermal condensation under 1 sun irradiation with 10 % of 2-propanol solution.

4.4. Conclusion

In summary, highly photoactive organic photocatalyst, g-C_3N_4, was synthesized through ionothermal method with KCl and LiCl salt. This synthesis process enhanced the low crystallinity of g-C_3N_4. Accelerated polymerization of g-C_3N_4 by molten-salt helped the g-C_3N_4 to improve condensation, and to get fewer defects. Compared to bulk synthesis, ionothermal synthesis dramatically increased photoactivity. Nevertheless, poor surface property of g-C_3N_4 inhibit the H2O2 generation in absence of 2-propanol. It may be improved by some strategies such as co-catalyst loading. On the other hand, decomposition rate of H_2O_2 of bulk and crystalline g-C_3N_4 didn't show much difference. However, their degradation rates itself were very low compared to other photocatalyst such as TiO_2. After quantity optimization of g-C_3N_4, H_2O_2 concentration was close to 20 mM at 24 h in 1 sun irradiation in presence of electron donor (2- propanol). Further researches and characterization will be carried out. For example, FT-IR spectra, morphological images, EDS and XRD patterns of two samples will be analyzed for comparison of crystalline structures and chemical bond difference. In addition, $BiVO_4$ and carbon nitride composite can be synthesized for water splitting because the $BiVO_4$ is a suitable photocatalyst for water oxidation to oxygen gas and carbon nitride is suitable for hydrogen evolution reaction.

4.5 Reference

[1] Yun Zheng, Lihua Lin, Bo Wang, and Xinchen Wang. *Angew. Chem. Int. Ed.* **2015**, 54, 12868–12884

[2] X. Wang , K. Maeda , A. Thomas , K. Takanabe , G. Xin , J. M. Carlsson , K. Domen and M. Antonietti , *Nat. Mater.*, **2009**, 8 , 76 -80

[3] Amene Naseri, Morasae Samadi, Ali Pourjavadi, Alireza Z. Moshfegh and Seeram Ramakrishna J. *Mater. Chem. A*, **2017**, 5, 23406

[4] Imran Majeed, Uzma Manzoor, Fehmida K. Kanodarwala, Muhammad Amtiaz Nadeem, Ejaz Hussain, Hassan Ali, Amin Badshah, John Arron Stride and Muhammad Arif Nadeem,. *Catal. Sci. Technol*., **2018**, 8, 1183–1193

[5] Xinchen Wang, Siegfried Blechert, and Markus Antonietti. *ACS Catal*. **2012**, 2, 8, 1596-1606

[6] Jingrun Ran, Tian Yi Ma, Guoping Gao, Xi-Wen Du and Shi Zhang Qiao. *Energy Environ. Sci.*, **2015**, 8, 3708

[7] Yajun Zhou, Lingxia Zhang, Weimin Huang, Qinglu Kong, Xiangqian Fan, Min Wang, Jianlin Shi,. *Carbon 99.* **2016**, 111-117

[8] Jinshui Zhang, Mingwen Zhang, Rui-Qing Sun, Xinchen Wang. *Angew. Chem. Int. Ed*. **2012**, 51, 10145 –10149

[9] Fang He, Gang Chen, Yaoguang Yu, Sue Hao, Yansong Zhou, and Yi Zheng, *ACS Appl. Mater. Interfaces.* **2014**, 6, 10, 7171-7179

[10] Qiuling Tay, Pushkar Kanhere, Chin Fan Ng, Shi Chen, Sudip Chakraborty, Alfred Cheng Hon Huan, Tze Chien Sum, Rajeev Ahuja, and Zhong Chen, *Chem. Mater*. **2015**, 27, 4930−4933

[11] Yasuhiro Shiraishi, Shunsuke Kanazawa, Yoshitsune Sugano, Daijiro Tsukamoto, Hirokatsu Sakamoto, Satoshi Ichikawa, and Takayuki Hirai, *ACS Catal.* **2014**, 4, 3, 774-780

[12] Shuna Li, Guohui Dong, Reshalaiti Hailili, Liping Yang, Yingxuan Li, Fu Wang, Yubin Zeng, and Chuanyi Wang, *Applied Catalysis B: Environmental.* **2016**, 190, 26–35

[13] Michael J. Bojdys, Jens-Oliver Müller, Markus Antonietti, Arne Thomas. *Chem. Eur. J*.**2008**, 14, 8177 – 8182

[14] Guigang Zhang, Guosheng Li, Zhi-An Lan, Lihua Lin, Aleksandr Savateev, Tobias Heil, Spiros Zafeiratos, Xinchen Wang, Markus Antonietti . *Angew. Chem. Int. Ed.* **2017**, 56, 13445–13449

[15] Han Zou, Xuehua Yan, Jie Ren, Xiao Wu, Yu Dai, Dawei Sha, Jianmei Pan, Jun Liu. *J Materiomics*. **2015**, 1, 340-347

[16] X. Liu, N. Fechler, M. Antonietti, *Chem. Soc. Rev*. **2013**, 42, 8237–8265

[17] Gerardo Algara-Siller, Nikolai Severin, Samantha Y. Chong, Torbjörn Björkman, Robert G. Palgrave, Andrea Laybourn, Markus Antonietti, Yaroslav Z. Khimyak, Arkady V. Krasheninnikov, Jürgen P. Rabe, Ute Kaiser, Andrew I. Cooper, Arne Thomas, and Michael J. Bojdys. *Angew. Chem.* **2014**, 126, 7580 –7585

[18] Lihua Lin, Zhiyang Yu, and Xinchen Wang, *Angew. Chem. Int. Ed*. 10.1002/anie.201809897

[19] Dariya Dontsova, Sergey Pronkin, Marko Wehle, Zupeng Chen, Christian Fettkenhauer, Guylhaine Clavel, and Markus Antonietti. *Chem. Mater*. **2015**, 27, 5170−5179

[20] Fabian K. Kessler, Yun Zheng, Dana Schwarz, Christoph Merschjann, Wolfgang Schnick, Xinchen Wang & Michael J. Bojdys. *Nature Reviews Materials*. **2017**, 2, 17030

[21] Sungeun Yang, Jiwhan Kim, Young Joo Tak, Aloysius Soon, and Hyunjoo Lee. *Angew. Chem. Int*. Ed. **2016**, 55, 2058 –2062

[22] Chang Hyuck Choi, Minho Kim, Han Chang Kwon, Sung June Cho, Seongho Yun, Hee-Tak Kim, Karl J.J. Mayrhofer, Hyungjun Kim and Minkee Choi. *Nature Communications.* **2016**, 7, 10922

5. Summary

Hydrogen peroxide is eco-friendly oxidizing materials that can be used in various fields such as a bleaching agent, disinfectant, and chemical synthesis. The worldwide consumption of hydrogen peroxide is increasing but the AO process which is conventional H_2O_2 synthesizing process contains several problems although the yield of H_2O_2 is high. It requires explosive H_2/O_2 gas mixture, large energy input, noble palladium metal catalyst and solution regeneration process due to byproduct formation. However, photocatalytic hydrogen peroxide generation can be a solution to those problems. It doesn't need explosive hydrogen gas, expensive noble metals such as palladium and hydrogen peroxide can be generated from earth-abundant materials that are only sun light, water, and oxygen. However, photogenerated hydrogen peroxide can be degraded by holes from Photocatalyst. Thus, maintaining a high concentration of hydrogen peroxide is one goal as well as generating it with high yield.

In here, three photocatalysts that can generate a high concentration of hydrogen peroxide under visible light are introduced. In **Chapter 2**, polymer/TiO_2 heterojunction photocatalyst is synthesized. The polymer consists of fluorene and benzothiadiazole unit and is called PFBT. Heterojunction helps to absorb a wider range of solar spectrum corresponding to the visible light region and to separate electron-hole pairs and reduce its recombination. Compared to bare TiO_2 photocatalyst, PFBT/TiO_2 heterojunction generates more than 45 times higher concentration of hydrogen peroxide. Moreover, hydrophobic characteristics from the polymer perform a key role in avoiding decomposition of hydrogen peroxide. To synthesize more hydrophobic polymer, fluorination of polymer was conducted. PFFBT polymer was synthesized by addition of one F atom at benzothiadiazole in polymer unit and PF2FBT polymer was synthesized by addition of two F atoms. Their hydrophobic nature was confirmed through measuring contact angles between polymers or polymer/TiO_2 composite and both water and hydrogen peroxide and it is proved that fluorination makes the polymer be hydrophobic and make less attraction with both H_2O and H_2O_2. Degradation performance of polymer/TiO_2 heterojunctions also tested. Bare TiO_2 degraded hydrogen peroxide the fastest while it generated hydrogen peroxide with the least amount. Addition of F atom in the polymer unit makes polymer be hydrophobic and decompose less amount of hydrogen peroxide compared untreated polymer. Heterojunction with two F atom-containing a polymer, PF2FBT, was the most hydrophobic and decomposed the least amount of hydrogen peroxide. However, the concentration of generated hydrogen peroxide was found to be similar in two cases where one fluorine atom was added

and two fluorine atoms were added in polymer although the value was much higher than pristine polymer/TiO_2 heterojunction. The reason for the results was originated from the broadest band gap and fast recombination of PF2FBT. Nevertheless, compared to bare TiO_2, about 80 times higher concentration of hydrogen peroxide was generated by both PFFBT/TiO2 and PF2FBT/TiO2 heterojunctions.

In **Chapter 3**, MOF-derived carbon@CdS composite photocatalyst is introduced. The MOF can be used as both template and precursor. As the CdS photocatalyst is synthesized from the MOF structure that contains cadmium and sulfur atoms by annealing at the high temperature, a carbon matrix is formed on the surface of the photocatalyst by carbonization of the organic ligands of the MOF at the same time. The destruction of the MOF structure was found by XRD pattern of MOF-derived samples with different annealing time and transformation from the MOF to single phase CdS was observed. The MOF structure still remains for 6 hours of annealing at 270 ^{O}C but for longer than 12hours of annealing let the MOF be fully-disappeared. The presence of carbon of the MOF-derived CdS is confirmed by EDS mapping and elemental analysis. Besides, it was confirmed that sulfur was doped in the carbon by XPS analysis. The carbon matrix on the surface of the photocatalyst plays the main role in inhibiting the decomposition of hydrogen peroxide and reducing recombination by separating electron-hole pairs rapidly. Optimized MOF-derived CdS produces more than 2mM of hydrogen peroxide in the absence of hole scavenger under visible light irradiation and it is 4.1 times higher value than a concentration of hydrogen peroxide generated by commercialized CdS for 3h of photo-reaction. To clarify the role of the carbon matrix, commercial CdS was treated under the same condition with MOF-derived CdS. Commercial CdS that thermally treated doesn't include carbon matrix because the carbon of MOF-derived CdS originated from the carbonization of the organic ligand. Then, we verified that if there was no carbon matrix on the CdS surface, its performance doesn't improve as much as MOF-derived CdS. From the hydrogen peroxide decomposition test, it is confirmed that MOF-derived carbon@CdS photocatalyst also shows slow decomposition rate compared to commercial CdS under visible light irradiation although H_2O_2 generation ability under visible light condition is much better than that of commercialized CdS. Moreover, MOF-derived carbon@CdS didn't saturate for 24 hours of performance test while commercial one was already saturated from 8 hours of the reaction and the concentration difference was increased to 6.3 times compare with commercial CdS at 24h.

In **Chapter 4**, graphitic carbon nitride photocatalyst synthesized through ionothermal reaction is introduced. The graphitic carbon nitride is one of the organic semiconductors that doesn't contain metal. Thus, it is considered as an eco-friendly and non-toxic photocatalyst. However, organic

photocatalysts suffer from low photoactivity due to strong exciton binding energy compared to inorganic materials. In addition, usual synthesis method, thermal condensation, for g-C_3N_4 is hard to synthesize crystalline materials because it is bulk polymerization and incomplete polymerization makes amorphous or semi-crystalline g-C_3N_4. To enhance a photoactivity by improving the crystallinity of the g-C_3N_4, ionothermal synthesis was applied. Ionothermal polymerization (a.k.a. molten-salt method) makes graphitic carbon nitride be more crystalline and structure be changed from heptazine-based to triazine based by residual salt. Moreover, compared to thermal condensation synthesis, ionothermal synthesis increases the photoactivity to produce hydrogen peroxide dramatically. The final concentration of hydrogen peroxide generated by ionothermal synthesis of graphitic carbon nitride was around 16 mM and this value is 6.2 times higher value of graphitic carbon nitride by thermal condensation under visible light with 10% 2-propanol solution. Although decomposition ability for hydrogen peroxide was almost the same for both cases, decomposition rate is slower than other types of photocatalyst such as TiO_2 even under 1 sun irradiation. However, its surface property was immensely poor so it was hard to generate H_2O_2 without hole scavenger. On the other hand, H_2O_2 concentration can be grown by optimizing the concentration of the catalyst. Although production rate per weight per time has trends that are reduction with an increase of the concentration, the highest H_2O_2 concentration is found at 1.6 g/L. in addition, its activity of quantity-optimized g-C_3N_4 was compared under both 1 sun and visible light. 1 sun irradiation let g-C_3N_4 utilize UV range of light spectrum and thus, the concentration of H2O2 increased from 7.87 mM in vis-light to 12.45 mM in 1 sun condition at 3 h. After 24 h of reaction, a dramatic increase to 19.6 mM was observed.

Acknowledgement

대학원에 입학하기 전부터 지금까지 2 년이 넘는 시간 동안 저를 이끌어주신 장지욱 지도교수님께 가장 먼저 감사의 인사를 드립니다. 처음으로 입학한 대학원생이라 모르는 것도 많고 답답한 부분도 있었을 텐데 실험과 실험실 생활의 전반적인 분야에 대해 조언과 격려를 아끼지 않으시고 지지해 주셔서 진심으로 감사합니다. 또한, 바쁘신 일정에도 불구하고 제 학위 논문 심사에 기꺼이 참석해주시고 공동연구의 기회를 주신 문회리 교수님과 양창덕 교수님께도 감사의 말씀을 드립니다. 마찬가지로 공동연구의 기회를 주시고 시뮬레이션 연구를 도와주시는 곽상규 교수님께도 감사드립니다.

제 학위 과정 동안 함께 연구를 진행한 모든 대학원생분들과 연구원분들께도 감사드립니다. 문회리 교수님 연구실의 이재화 대학원생, 양창덕 교수님 연구실의 조용준 대학원생, 곽상규 교수님 연구실의 고은민 대학원생, 박성오 대학원생, 그 외 연구에 도움을 주신 모든 분 덕분에 의미 있는 결과를 낼 수 있었습니다. 정말 감사합니다.

JW Energy Lab 의 박사님과 친구, 후배들에게도 감사의 말을 전합니다. 제가 논문과 학위논문을 작성하고 디펜스 발표 자료 만들 때 많은 도움을 주신 Sharma 박사님께 진심으로 감사드립니다. 바쁠 텐데도 제 후속 연구를 진행하기 위해 노력해주는 고마운 현진이와 좋은 의견을 많이 제안해 준 묘화, 의논 상대가 되어준 창환이와 의욕적이고 열정 넘치는 동락이, 똑 부러지는 제민이, 함께한 시간은 짧았지만 언제나 친절한 Rashmi 에게도 고맙다는 말을 전합니다. 착하고 똑똑하고 성실한 친구들 덕분에 대학원 생활을 하는 동안 즐겁게 보낼 수 있었습니다.

고등학교 은사님이신 김종욱 선생님께도 이 자리를 빌려 감사를 마음을 정합니다. 선생님 덕분에 고등학교 시절을 잘 넘길 수 있었습니다. 더불어 항상 곁에서 응원해준 대학 동기 지희, 보연이, 동은이, 예진이, 원식이, 민곤이, 혁진이와 오랜 친구들 슬비, 성혜, 정현이, 은혜, 은아, 예진이에게도 고맙습니다. 힘들 때마다 격려해준 형개 선배와 룸메이트 수민이도 고맙습니다.

마지막으로, 언제나 제 의견을 존중해 주시고 저를 아끼고 응원하고 지지해준 부모님과 가족, 친척분들께 감사의 말씀을 드립니다.